Bioactive Materials 21 (2023) 110–128

Contents lists available at ScienceDirect

Bioactive Materials

journal homepage: www.keaipublishing.com/en/journals/bioactive-materials

A novel decellularized matrix of Wnt signaling-activated osteocytes accelerates the repair of critical-sized parietal bone defects with osteoclastogenesis, angiogenesis, and neurogenesis

Xiaofang Wang [a,1], Yufei Ma [a,1], Jie Chen [a,1], Yujiao Liu [a,1], Guangliang Liu [a], Pengtao Wang [a], Bo Wang [a], Makoto M. Taketo [b], Teresita Bellido [c], Xiaolin Tu [a,d,*]

[a] Laboratory of Skeletal Development and Regeneration, Institute of Life Sciences, Chongqing Medical University, Chongqing, 400016, China
[b] Department of Pharmacology, Graduate School of Medicine, Kyoto University, Kyoto, 606-8501, Japan
[c] Department of Physiology and Cell Biology, University of Arkansas for Medical Sciences, Little Rock, AR, 72223, USA
[d] Department of Anatomy and Cell Biology, Indiana University School of Medicine, Indianapolis, IN, 46202, USA

ARTICLE INFO

Keywords:
Decellularized matrix
Osteocyte
Wnt signaling
3D printing
Regenerative repair
Metabolic and neurovascular organoid bone

ABSTRACT

Cell source is the key to decellularized matrix (DM) strategy. This study compared 3 cell types, osteocytes with/without dominant active Wnt/β-catenin signaling (daCO and WTO) and bone marrow stromal cells (BMSCs) for their DMs in bone repair. Decellularization removes all organelles and >95% DNA, and retained >74% collagen and >71% GAG, maintains the integrity of cell basement membrane with dense boundaries showing oval and honeycomb structure in osteocytic DM and smooth but irregular shape in the BMSC-DM. DM produced higher cell survival rate (90%) and higher proliferative activity. In vitro, daCO-DM induces more and longer stress fibers in BMSCs, conducive to cell adhesion, spreading, and osteogenic differentiation. 8-wk after implantation of the critical-sized parietal bone defect model, daCO-DM formed tight structures, composed of a large number of densely-arranged type-I collagen under polarized light microscope, which is similar to and integrated with host bone. BV/TV (>54%) was 1.5, 2.9, and 3.5 times of WTO-DM, BMSC-DM, and none-DM groups, and N.Ob/T.Ar ($3.2 \times 10^2/mm^2$) was 1.7, 2.9, and 3.3 times. At 4-wk, daCO-DM induced osteoclastogenesis, 2.3 times higher than WTO-DM; but BMSC-DM or none-DM didn't. daCO-DM increased the expression of *RANKL* and *MCSF, Vegfa* and *Angpt1*, and *Ngf* in BMSCs, which contributes to osteoclastogenesis, angiogenesis, and neurogenesis, respectively. daCO-DM promoted H-type vessel formation and nerve markers β3-tubulin and NeuN expression. Conclusion: daCO-DM produces metabolic and neurovascularized organoid bone to accelerate the repair of bone defects. These features are expected to achieve the effect of autologous bone transplantation, suitable for transformation application.

1. Introduction

Bone tissue has the ability of self-repair and regeneration, but the critical-sized bone defect caused by trauma, tumor, or infection cannot heal itself. Surgery with bone transplantation is needed for these patients [1]. Autologous bone transplantation is considered as the "gold standard" for bone repair due to its excellent features of osteogenesis, histocompatibility, high bone healing rate, and complete bone fusion. However, there are still limitations such as restricted source and risk of donor site complications [2]. Most of the bone repair materials in the huge existing market are metal, ceramic, and polymer materials etc [3]. However, these materials have insufficient bioactivity and difficult shape matching of individual bone, resulting in low ability in bone regeneration, loosening, and transplantation failure. Therefore, the second surgery for implant revision will inevitably be carried out within 5–20 years after operation [4,5].

The invention of hard material and cell integrated 3D bioprinting technology [6,7] has successfully realized the personalized adaptation

Peer review under responsibility of KeAi Communications Co., Ltd.
* Corresponding author. Laboratory of Skeletal Development and Regeneration, Institute of Life Sciences, Chongqing Medical University, Chongqing, 400016, China.
E-mail address: xtu@cqmu.edu.cn (X. Tu).
[1] These authors contributed equally to this work.

https://doi.org/10.1016/j.bioactmat.2022.07.017
Received 8 April 2022; Received in revised form 21 June 2022; Accepted 14 July 2022

of hard material scaffolds with mechanical support, creating a suitable biological microenvironment for cell adhesion, proliferation, and differentiation, so as to meet the challenges faced by orthopedic materials. However, the application of exogenous living cells still has the limitations of ethical supervision and approval, standardized technology, and high cost, as well as the deficiencies of cell survival rate, proliferation, function maintenance, and rejection [8–10].

The cell-free strategy represented by decellularized matrix (DM) may solve the above-mentioned issues [11]. DM is a natural fiber network composed of proteins, glycosaminoglycans, and proteoglycans etc., produced by cells with the natural configuration of tissue-specific three-dimensional pattern, inherent characteristics, and interactions of biological factors. Thus, DM can help target tissues/organs to maintain specific activities in structural support, migration, adhesion, proliferation, and differentiation of cells to provide a naturally stable internal environment for development, even recruits endogenous stem cells/progenitor cells to repair and regenerate damaged tissues [12]. DM can be obtained from either tissues/organs or cell culture in vitro. The tissue/organ-based DM easily keeps the structure and biological activity of natural bone tissue to effectively promote bone regeneration. However, its sources and application are as limited as autogenous bone graft [13]. Therefore, cell-derived DM has become a research hotspot. In addition, cell-derived DM can be modified to the surface of orthopedic materials, such as hydroxyapatite, biphasic calcium phosphate and polymers, which can be easily transformed for application [14]. Thus, the development of cell-derived DM as a bioactive material is expected to fabricate cell-free scaffolds with bionic microstructure and microenvironment, which will break the bottleneck of existing bone repair materials and reach the "gold standard" of autologous bone repair.

The core content of DM research is the selection of cell source and how to realize its developmental function [15]. Tissues/organs are composed of multiple cells [16–18]. Can one type or combined many types of cells simulate the naturally-stable internal environment, which overcomes inflammatory environment and plays a specific role in development after implantation? Kohn et al. found that the DM of bovine primary chondrocytes and osteoblasts induces the differentiation of human mesenchymal stem cells (MSCs) into chondrocytes and osteoblasts, respectively [19]. Pati et al. reported that the PCL/PLGA/β--tricalcium phosphate scaffolds, modified with the DM of mineralized extracellular matrix originally from hMSCs, enhances the adhesion, proliferation, differentiation, and mineralization of hMSCs. Eight weeks after implantation into a rat parietal critical bone defect, the amount of formed bone induced by the DM-modified scaffolds is twice that of the control group [20]. However, the clinical application of hMSCs is restricted by limited sources and heterogeneity of MSCs [21], and the aging or growth stagnation period that MSCs may enter after 24–40 amplification in vitro [22]. Needless to say, MSCs need to be induced into differentiated cells with mineralized matrix in vitro before obtaining a good osteogenic microenvironment. These issues are unfavorable for the application of MSCs [18]. Thus, bone cells, including pre-osteoblasts, osteoblasts, and abundant osteocytes, may have more specificity, inducibility, and practicability than stem cells [19].

Lee et al. modified 3D printed porous collagen scaffolds with the DM of murine pre-osteoblastic cell line MC3T3-E1 to significantly improve cell proliferation, osteogenic differentiation, and mineralization activities, suggesting that pre-osteoblast DM could be a bone tissue repair material with good biocompatibility [23]. Unfortunately, its bone repair ability has not been evaluated in that study. Ma et al. cultured MC3T3-E1 overexpressed LMP-1 gene on calcined bovine bone for 7, 14, and 21 days respectively to generate three DM composite scaffolds. Although no significant difference in the amount of new bone formed among the groups within 8 wk after implantation in New Zealand rabbits; at 12-wk, the composite scaffolds of 7-day culture better promote the repair of bone defects with highest BV/TV (50%) than the other two scaffolds cultured for 14 days (30%) and 21 days (40%). The reason is that the latter two scaffolds caused persistent inflammation of the host, which hinders bone regeneration [24]. Therefore, the length of cell culture time affects the function of DM. More important, Aldemir Dikici et al. used abundant osteocytes of terminally-differentiated cell type in bone development to prepare osteocytic cell line MLO-A5 DM for the modification of 3D-printed PCL scaffolds, they found that the osteocytic DM has dual functions of bone formation and angiogenesis in vitro [25]. But it is also necessary to evaluate the function of osteocytic DM on bone repair after implantation.

It can be seen from the above studies that the naturally-stable internal environment required for development depends on the selection of cell type and culture time etc. DM from osteoblast lineage cells well induces the development of osteoblasts and blood vessels. However, it is still necessary to find cells that can induce bone formation and resorption as natural bone does. However, DM induction of osteoclastogenesis has not been reported. Based on our best knowledge, one or more cells that regulate bone development in this regard has not been reported. The DM with bone formation, bone resorption, and blood vessel and nerve formation is the key to the fabrication of bionic multifunctional DM, so as to regulate bone development in vivo and realize the function of genuine bone, such as metabolism (anabolism and catabolism), vascularization, and neuralization.

Bone development is a highly coordinated process involving the interaction between a variety of cell types present in bone tissue, including osteocytes, osteoblasts, osteoclasts, fibroblasts, endothelial cells, and immune cells [26]. Studies have shown that osteocytes communicate with osteoclasts and osteoblasts through RANKL/OPG [27,28] and SOST/Wnt [29–31], and coordinate their activities on bone surface, controlling the remodeling and regeneration of bone in vivo [32]. The classical Wnt signaling pathway has a great influence on osteogenesis [33,34]. We seminally found that activation of canonical Wnt signaling in murine osteocytes mediates bone anabolism with unexpected bone resorption [35] as a physiological role of intrinsic bone [36,37]. In addition, we proved that osteocytes are the target cells of osteogenic parathyroid hormone(PTH)because mice lacking PTH receptors in osteocytes lose their osteogenic response to PTH intermittent therapy [38]. Furthermore, we found that Wnt agonist activated osteocytic cell line MLO-Y4 promotes osteogenic differentiation and angiogenesis [39], and primary osteocytes with dominant active Wnt signaling can significantly promote the differentiation of BMSCs torwards osteoblast and induces natural osteogenesis in a 3D-printed PCL module with osteoclastogenesis and neurovascularization (submitted for publication). Therefore, we hypothesized that osteocyes, which account for more than 90% of the total number of bone cells, produces osteogenic microenvironment for bone development after Wnt signaling activation, and as the ideal cell type to biofabricate osteogenic DM to repair defects as the development of nature bone.

In this study, we used primary osteocytes with dominant-active Wnt/β-catenin signaling (daCO), compared with wild-type osteocytes (WTO) and BMSCs, a cell type commonly used in bone tissue engineering, and prepared decellularized matrix-modified 3D printed PCL as functional modules. We compared their function on cell survival, adhesion, spreading, proliferation, and osteogenic differentiation ex vivo. Furthermore, a mouse parietal critical-sized bone defect model was used to evaluate bone regeneration, osteoclastogenesis, and neurovascularization by the daCO-DM. The results indicated that the daCO-DM module, as a novel bioactive biomaterial, may has multifunction as natural bone, which can be called artificial organoid bone [40]. It is expected to achieve the effect of autologous bone transplantation as dreamed in clinical application.

2. Materials and methods

2.1. Animals

The mice with Wnt signaling activated in osteocytes (daβcat^{Ot}) and its wild type control mice (WT) were generated as previously reported

[35]. Briefly, DMP1-8 kb-Cre mice, which express Cre recombinase in osteocytes, but not in osteoblasts [41] was crossed with $Catnb^{lox(ex3)/lox(ex3)}$ mice, in which exon 3 that encodes for the sites required for β-catenin degradation is flanked by LoxP sites [42]. All animal procedures were approved by the Institutional Animal Care and Use Committee of Chongqing Medical University.

2.2. Materials

2.2.1. Chemicals

RIPA lysis buffer, Polycaprolactone (PCL, average MW 45000), collagenase type IA, Alizarin Red S, and cetylpyridinium chloride were purchased from Sigma-Aldrich (St Louis, MO, USA), Trizol from Acurate Biology (Hunan, China), DNase from Solarbio Biotechnology (Beijing, China). Avertin from Aibei Biotechnology CO., Ltd (Nanjing, China), cytochalasin D from Med Chem Express (Shanghai, China), MCSF and RANKL from Novoprotein Biotechnology CO., Ltd (Suzhou, China).

2.2.2. Assay kits

Quant-iT™ PicoGreen® dsDNA reagent kit, Vybrant DiO cell-labeling solution, and LIVE/DEAD cell viability kit were purchased from Invitrogen (Carlsbad, CA, USA), Hochest 33258 nuclear staining solution from Solarbio Biotechnology (Beijing, China). Conventional hydroxyproline assay kit from Jiancheng Biotechnology (Nanjing, China). Alcian blue colorimetry in total glycosaminoglycan (GAG) content kit from GENMED (Wilmington, DE, USA). Rhodamine-Phalloidin cytoskeleton staining solution from Cytoskeleton Inc (St. Denver, CO, USA). BCIP/NBT alkaline phosphatase (AP) color development kit, AP assay kit, and bicinchoninic acid (BCA) protein assay kit from Beyotime Biotechnology (Shanghai, China), cell counting kit-8 from Dojindo (Kumamoto, Japan), reverse transcription kit and real-time fluorescent quantitative PCR kit from Acurate Biology (Hunan, China), Acid Phosphatase, Leukocyte (TRAP) Kit from Sigma-Aldrich (St Louis, MO, USA).

2.2.3. Reagents of cell culture

Fetal bovine serum (FBS) and α-minimum essential medium (α-MEM) were obtained from Gibco (Maryland, Gaithesburg, USA), pancreatin and penicillin/streptomycin (PS) from Beyotime Biotechnology (Shanghai, China).

2.2.4. Antibodies

Anti-CD31 antibody was supplied from Servicebio (Wuhan, China). Anti-β3-Tubulin antibody and anti-Endomucin antibody from Affinity Biosciences LTD (Guangzhou, China). Anti-NeuN, Anti-NGF, Anti-VEGF antibody from Abcam Biotechnology (Shanghai, China).

2.3. Cell culture

2.3.1. Isolation and culture of BMSCs

BMSCs were isolated according to a previous study [43]. Briefly, the femurs of 8-week-old C57BL/6 male mice were dissected. After removing the metaphysis of the femur, the bone marrow was flushed out with α-MEM. Then the resulting α-MEM/bone marrow mixture was centrifuged at 800 rpm for 5 min.The cells in the centrifuge tube were resuspended with 1 mL growth medium (89% α-MEM, 10% FBS, and 1% PS) and cultured in an incubator (5% CO_2, 37 °C). The half medium was changed once every 2 or 3 days. The BMSCs were passed once at day 7 or 8 after culture. The 2nd passage of BMSCs were used in experiments.

2.3.2. Isolation and culture of osteocytes

The osteocytes were isolated from the tibiae and femurs of 8-week-old $da\beta cat^{Ot}$ male mice and its wild-type controls as previously described [44] with modification. In brief, after the metaphysis of the femur removed, followed by flushing the marrow cavity with 1 mL a-MEM for 3 times. The bone were cut into 1 mm^3 pieces and digested by 1 mg/mL collagenase type IA solution at 37 °C for 15 min (repeat three times). The digested bone pieces were reciprocally treated by the collagenase solution 15 min and ethylenediamine-tetra acetic acid solution (EDTA 4 mM, pH7.4) 5 min for three times. And then, the bone fragments were cultured in growth medium in incubator (5% CO_2, 37 °C, 95% humidity). After culture for 3 days or more, the cells migrated out of the digested bone fragments. The osteocytes isolated from wild-type male mice were named WTO, and the osteocytes isolated from $da\beta cat^{Ot}$ male mice were named daCO hereafter.

2.3.3. Isolation and culture of bone marrow mononuclear cells (BMMs)

BMMs were isolated from bone marrow cells as described [45]. Briefly, the bone marrow cells were cultured in 100 mm-cell culture dish with 10 mL culture medium of 10% FBS, α-MEM and 30 ng/mL MCSF for 3 days, then the suspending cells was collected and centrifuged at 200×*g* for 3 min, the cells in the pellet were resuspended in 1 mL culture medium and used as BMMs for osteoclastogenesis assay.

2.4. Biofabrication of DM modified 3D-printed PCL scaffold

2.4.1. PCL 3D printing

PCL was used to print modules by a 3D bioprinter according to a predesigned 3D scaffold model by STL standardized file format [6]. PCL scaffolds sized 5 × 5 × 1 mm with strand width 300 μm and pore size 400 μm were printed for in vitro experiments. For in vivo experiments, a 5 × 5 × 0.4 mm scaffold was printed with the same width and pore size, and then cut into a circular scaffold with a diameter at 4.5 mm. Studies have confirmed that pore size of 3D-printed scaffolds about 500 μm can effectively promote blood vessel formation and new bone formation [46].

2.4.2. Cell culture on 3D-printed PCL scaffold

The procedures of cell culture on 3D-printed PCL scaffold were slightly modified as described in a previous study [47]. Briefly, the modules were immersed in 75% alcohol for 1 h, washed in sterile phosphate buffer (PBS) 5 times for 3 min each. Then the scaffolds were placed on a clean bench to dry and irradiated under UV light for 20 min on both top and bottom of the scaffolds. Next, 10 μL FBS was added to every scaffold for infiltration. The expanded cells were seeded on the scaffold by adding 10 μL of cell suspension solution (2×10^7 cells/mL) in each scaffold in a 24-well plate and cultured in an incubator (37 °C, 5% CO_2). After cultured for 2 h, 1 mL growth medium was added in each well for cells growing on the modules. The medium was replaced every two days.

2.4.3. Determination of cell cultured time for decellularization

Cells marked with green fluorescence Dye were cultured on modules for 1, 4, 7, 10, and 14 days respectively. Then the cells were lysed with 500 μL RIPA lysis buffer for 5 min on ice. The lysed cell suspension was centrifuged at 12,000 rpm for 3 min, and the supernatant was measured for quantifing the protein accumulated on the scaffold by BCA protein assay kit [48].

2.4.4. Decellularization of the cells on 3D-printed PCL scaffold

DM-modified 3D-printed PCL modules were obtained after freeze-thaw cycling and DNase I treatment as described in a previous study [25]. Briefly, the cell-seeded modules were cultured for 14 days and then the growth medium was discarded. After washed twice with sterile PBS, the modules were transferred to 15 mL centrifuge tubes and 500 μL of sterile PBS was added in each tube. Then, the tubes were snap frozen in liquid nitrogen for 10 min and subsequently thawed at 37 °C in a water bath for the next 10 min. This freeze-thaw cycling was performed 3 times. The treated modules were immerged in sterile PBS 3 times (3 min/time) to remove cell debris. Finally, the modules were incubated in 500 μL 0.2 mg/mL DNase I solution at 37 °C for 1 h and stored in sterile PBS at 4 °C. The DM modified 3D-printed PCL modules were in a clean

bench, and followed by the irradiation of UV light on the tops and bottoms of these modules for 10 min each side before use.

2.5. Characterization of DM-modified 3D-printed PCL modules

2.5.1. Scanning electron microscopy

Scanning electron microscope (SEM) was used to characterize the surface topography of the modules as reported [20]. The modules were fixed with 2.5% glutaraldehyde in PBS for 1h, and then dehydrated successively in 70%, 90%, 95%, and 100% ethanol for 15 min each. The fixed modules were vacuum dried, sputter-coated with gold, then examined with scanning electron microscope (Hitachi, Tokyo, Japan) operated at 10 kV.

2.5.2. Evaluation of DM components

DM-modified modules were evaluated for DNA, collagen, and GAG as reported [20,49]. The total DNA was quantified by the dsDNA reagent kit. The fluorescence intensity was measured using a fluorescence spectrophotometer (Leica, Wetzlar, Germany) at excitation wavelength 480 nm and emission wavelength 520 nm to assess the amount of DNA within the modules. The Hoechst 33258 was used to stain DNA remaining on the modules for evaluating DNA removal. The total collagen on the modules was determined by hydroxyproline assay kit according to the instructions. The absorbance was measured at 550 nm and quantified by referring to a standard curve made in advance with hydroxyproline. Alcian blue colorimetry in total GAG content kit was used for GAG assay and the absorbance was detected at 600 nm.

The expression of vascular endothelial cell growth factor (VEGF) and nerve growth factor (NGF) were detected by immunofluorescence (IF). In brief, scaffolds were permeabilized with 0.25% Triton-X100 for 20 min at room temperature, and respectively incubated with each antibody (1:50) of anti-VEGF, and anti-NGF overnight at 4 °C. Fluorescence-labelled secondary antibodies (1:100) were respectively incubated on the scaffolds at room temperature for 2 h, and then the stained sections were observed and photographed with fluorescence microscope (Leica, Wetzlar, Germany).

2.6. Cell biocompatibility of DM-modified 3D-printed PCL modules

Cell compatibility of DM derived from BMSCs (BMSC-DM), osteocytes of wild-type control mice (WTO-DM) and Wnt signaling-activated osteocytes of daβcat^{Ot} mice (daCO-DM) modified 3D-printed PCL modules was examined in cell viability, spreading, and proliferation compared to none-DM modified PCL modules (none-DM). BMSCs were seeded on each group of modules at 2×10^5 cells/module.

2.6.1. Cell viability

Cell viability was assessed by LIVE/DEAD™ cell viability assay as reported [39] in the cell culture on DM modified modules for 24 h. In short, the modules were stained by LIVE/DEAD staining mixture containing calcein AM (0.5 μL/mL) and ethidium-1 (EthD-1, 2 μL/mL) at room temperature for 1 h. Then, the modules were observed and taken pictures under fluorescence microscope (Leica, Wetzlar, Germany). Live and dead cells were exhibited green and red fluorescence under the microscope and calculated with ImageJ software (NIH, Bethesda, USA).

2.6.2. Cell spreading

F-actin staining was used to label cytoskeleton to evaluate cell adhesion and spreading as described [50]. The BMSCs were seeded on the modules and culture for 24 h. The cells were stained for F-actin with phalloidin-rhodamine and the nuclei were visualized with DAPI. After staining, the cell spreading was visualized under fluorescence microscope. Cell spreading area was measured by the active contours algorithm using ImageJ.

Cytochalasin D (CytoD) treatments: To explore the role of actin cytoskeleton in osteogenic differentiation, cytoskeleton depolymerization was induced by CytoD [51], an actin polymerization inhibitor. Briefly, 1 mg CytoD was initially dissolved in 1.97 mL dimethyl sulfoxide (DMSO) to make 1 mM storage solution. BMSCs were harvested and suspended with growth media, and then seeded on daCO-DM modified scaffolds with a cell density of 2×10^5 cells per scaffold. Growth medium was changed once every 3 days. After 7 days, 2 μM Cyto D was added in the medium and treated 1 h. F-actin staining, AP staining, and osteoblast marker genes expression were performed 7 days later.

2.6.3. Cell proliferation

Cell proliferation activity was measured by cell counting kit-8 assay on day 1, 4, and 7 after BMSCs seeded on the modules as reported [39]. The modules were washed with PBS and placed in a 96-well plate. A total of 10 μL CCK-8 solution in 100 μL PBS was added to each well, and then the plate was incubated at 37 °C for 1 h. Subsequently, the supernatant of each well was pipetted into a new 96-well plate and the absorbance was measured at 450 nm by using a microplate reader.

2.7. Ex vivo assays for osteogenesis in DM-modified 3D-printed PCL modules

2×10^5 BMSCs were seeded on DM-modified 3D-printed PCL modules and cultured for 7 and 14 days, respectively. Osteogenesis was measured by AP staining, AP biochemical activity assay, qPCR for the expression of osteoblast marker genes, and mineralization assay.

2.7.1. AP staining

AP staining was performed per instruction of the BCIP/NBT AP color development kit as reported with modification [39]. Briefly, after culture, the modules were washed with PBS, and fixed in 3.7% formaldehyde for 5 min at room temperature, followed by staining with the color solution of the kit for 30 min. The staining results was recorded by a digit camera (Nikon, Sendai, Japan).

2.7.2. AP biochemical activity assay

AP biochemical activity assay was carried out as previously described [39]. Briefly, 200 μL Tris-HCL (50 mmol/L, pH = 7.4) was added to each module. Then, the cells were sonicated for three times (30 s every time) on ice. After centrifugation, the supernatant was collected for total protein measurement by BCA protein assay kit and AP biochemical activity of its substrate according to the instruction of the AP assay kit. Finally, the relative activity of AP was calculated by AP biochemical activity and normalized by the amount of protein and the duration of reaction time.

2.7.3. Detection of gene expression

Total RNA extraction and quantitative PCR (qPCR) were performed to measure the expression of osteoblast marker genes, pro-osteoclastogenic cytokines, angiogenesis related and neurogenic genes as reported [35,39]. Briefly, total RNA was extracted by Trizol from the cells in the modules culture for 7 and 14 days. cDNA was synthesized by using high capacity cDNA reverse transcription kit (Acurate, Hunan, China) per manufacturer's instruction. The expression of osteoblast marker genes (*Alpl, Runx2, Col1a1, Bglap*) at 7 and 14 days, and pro-osteoclastogenic cytokines (*RANKL, MCSF*) at 14 days were detected by qPCR using primer sets as list in Table 1. Relative mRNA expression levels were normalized to the housekeeping gene *Gapdh* by using the ΔCt method [39].

2.7.4. Mineralization assay (alizarin red S staining)

The modules were cultured in growth medium for 7 days, and then bone nodule formation was induced in osteogenic medium containing 0.1 mM dexamethasone, 10 mM β-glycerophosphate disodium salt solution, and 50 μg/mL L-ascorbic acid for 14 days. Matrix mineralization was analyzed by alizarin red S staining [39]. The modules were stained

Table 1
Primers for quantitative Real-Time PCR.

Gene	Forward sequence (5′-3′)	Reverse sequence (3′-5′)
Alpl	TATGTCTGGAACCGCACTGAA	CACTAGCAAGAAGAAGCCTTT
Runx2	ATCCAGCCACCTTCACTTACA	GGGACCATTGGGAACTGATAG
Bglap	AACGGTGGTGCCATAGATGC	AGGACCCTCTCTCTGCTCAC
Col1a1	CAGGCTGGTGTGATGGGATT	CCAAGGTCTCCAGGAACACC
MCSF	CGCTGCCCTTCTTCGACAT	TCTGACACCTCCTTGGCAATACT
RANKL	TGAGCCTCCGAGCAGAACTGAC	CTGCCTGTGTAGCCATCTGTTGAG
Ngf	GGCTACTACCAGGACGAGGAGAC	TGGTTGGCTTCATCTGAGTATGTGC
Vegfa	GGGCTCTTCTCGCTCCGTAGTAG	CCCTCTCCTCTTCCTTCTCTTCCTC
Angpt1	TTGATCTTCGTGCTGGGTCTGG	CTCTGTAAGGGCTTCCATTCGC
Gapdh	AACTCCCATTCTTCCACCTTT	CTCTTGCTCTCAGTATCCTTG

with 0.4% alizarin red S solution for 30 min and taken pictures. Then, the modules were extensively washed with PBS at room temperature, and the stain solution was destained in 10% cetylpyridinium chloride for 1 h and the washing solution was measured for absorbance at 562 nm for quantitation of mineralization status.

2.7.5. Ex vivo assay for osteoclastogenesis in DM-modified 3D-printed PCL modules

2×10^5 BMMs in 15 μL of osteoclast differentiation medium containing 10% FBS and 100 ng/mL RANKL and 30 ng/mL MCSF in α-MEM [52] were seeded on DM-modified 3D-printed PCL modules and cultured for 2 h, and 500 μL of osteoclast differentiation medium was added in the 48-well plate and continue to culture for 5 days until the formation of osteoclast. The cell culture was fixed by 4% paraformaldehyde for 10 min at room temperature, washed with tape water and air dred until TRAP staining for the detection of osteoclastogenesis [53].

2.8. DM-modified 3D-printed PCL modules repair bone defects

2.8.1. Mouse critical-sized parietal bone defect model

For assessing the ability in bone regeneration, the modules were implanted in a mouse standard bone defect model (4.5-mm in diameter) [54]. In total, 20 male 8-week-old C57BL/6 mice weighing ~25.0 g were randomly divided into two groups (n = 10 each group) before operation. The mice were anesthetized with intraperitoneal injections of avertin (0.2 mL/10 g), and then positioned in a stereotaxic frame after lost reflex reaction and immobilized during surgery. A trephine (TUUME, Guangzhou, China) with an outer diameter of 4.5 mm was used to remove bone from the parietal bone. Each mouse received two 4.5-mm-diameter modules of either none-DM and BMSC-DM or WTO-DM and daCO-DM. Control groups include none-DM, BMSC-DM, and WTO-DM. The module was fixed with suture (5–0). After the operation, the mice were kept on the operating bed until they wake up and have free access to food and water thereafter. 4 and 8 weeks later after implantation, the mice were sacrificed by CO_2 asphyxiation and the parietal bone of the mice was harvested, fixed in 4% paraformaldehyde at 4 °C for 24 h.

2.8.2. PET-CT analysis

The parietal bone was subjected to radiographic analysis by a nanoScan PET/CT (MEDISO, Utah, USA) and three-dimensionally reconstructed with PMOD software at threshold of 550 (PMOD Technologies, Zurich, Switzerland) as reported [55,56]. The CT images of specimens were taken at a resolution of 50 μm at 50 kV and 560 μA. The regenerated bone was evaluated by bone area and its coverage in the defect site (tissue area) was calculatedfrom the 3D reconstructed images using ImageJ. New bone formation was evaluated by BA/TA.

2.8.3. Bone histomorphometry

After PET-CT analysis, all the parietal bones were immersed in 14% ethylenediamine tetraacetic acid solution (EDTA w/v in PBS, pH7.4) for 2 weeks' decalcification. The decalcified samples were dehydrated through a series of gradient concentration of ethanol, transparented by xylene, embedded in paraffin, and finally sectioned into 5 μm slices with a microtome (Leica, Wetzlar, Germany) as reported [35].

Static bone histomorphometric analysis was performed as usual. The formed bone area and the number of osteoblasts which were visualized in the sections of these four groups of modules by HE staining. The osteoblast number were calculated per tissue area (N.Ob/T.Ar) by the OsteoMeasure High Resolution Digital Video System (OsteoMetrics, Decatur, Georgia, USA) due to the fact that osteoblasts were distributed in the area where the bone was forming so that the osteoblasts have not resided on the formed bone surface.

Tartrate-resistant acid phosphatase (TRAP) staining was used to detect osteoclasts. The osteoclasts were formed and connected with each other, hard to count individual osteoclast number, so we counted osteoclast surface length. Due to the same fact above that the bone was still forming so that osteoclast number was normalized to bone area as Oc.S/T.Ar for the evaluating the function of the DM on osteoclastogenesis.

2.8.4. Evaluation of osteoblast activity

The paraffin sections were stained with Picrosirius red for observation of the formation of collagen I as previously described [57]. Collagen I is as a marker of osteoblast activity produced and secreted from osteoblast, which was bright red or yellow under inverted optical microscope, and yellow or red under polarized light microscope, with dense arrangement and strong birefringence.

2.8.5. Analysis of the formed vessels

The formed vessels were visualized in the sections of these four groups of modules by HE staining [58]. The number of vessels in the newly formed bone were calculated as vessel number per tissue area (N. Vessel/T.Ar) using the OsteoMetrics.

2.8.6. Detection of neurovascular markers

The expression of vascular markers CD31 and Endomucin, and neuronal differentiation makers β3-Tubulin and NeuN were respectively detected in vivo by immunofluorescence (IF) as reported [59–61]. In brief, paraffin sections were permeabilized with 0.25% Triton-X100 for 20 min at room temperature, and respectively incubated with each antibody (1:50) of anti-Endomucin, anti-CD31, anti-β3-Tubulin, and anti-NeuN overnight at 4 °C. Fluorescence-labelled secondary antibodies (1:100) were incubated on the labelled sections at room temperature for 2 h, and then the stained sections were observed and photographed with a confocal laser (Nikon, Sendai, Japan). The expression of angiogenesis related genes (*Vegfa* and *Angpt1)* and *neurogenic gene* (*Ngf)* after 14 days of BMSCs culturing on DM modifed scaffolds was detected by qPCR.

2.9. Statistical analysis

Statistical analysis was performed by GraphPad Prism 8.0 software. All quantitative data were presented as means ± standard deviation (SD). The difference between multiple groups and two independent variables was analyzed by using One Way ANOVA and Two Way

ANOVA, respectively. Furthermore, Brown-Forsythe and Welch ANOVA tests were used for correction analysis. Student's *t*-test was performed between two comparable groups. Nonparametric Kruskal-Wallis test was used to compare medians instead when data distributions are not normal. A P value < 0.05 was considered significance for all statistical tests. Each experiment was repeated at least three times independently.

3. Results

3.1. Isolation and growth of cells on 3D-printed PCL scaffolds

Scaffolds with pore size at 300–500 μm may promote the formation of blood vessel and new bone formation [62]. Therefore, in this study, we used a 3D printer to print a PCL scaffold with a size of 5 × 5 × 1 mm at scaffold strand diameter 300 μm and interval 400 μm between strands (Fig. 1a). The images taken by digital camera and scanning electron microscope (SEM) showed that the 3D-printed PCL scaffold display a smooth surface with a uniform shape of material strands and consistent pore size about 300–500 μm as pre-designed.

In order to evaluate the effect of DM from osteocytes with activated Wnt signaling on osteogenesis, we first isolated and cultured the osteocytes (daCO) from the long bones of the mice with dominant active β-catenin from daβcat^{Ot} mice [35]. The cultured daCO displayed a little bit swollen and bigger in size than WTO. Both types of osteocytes are smaller than BMSCs (Fig. 1b) as documented [32].

These osteocytes and BMSCs were seeded on the scaffolds at cell density of 2 × 10^5 cells/scaffold and cell growth were observed by labelling with Dio green dye at different days after culture. As shown in Fig. S1a, the number of cells with green fluorescence increased with the extension of culture time, suggesting a well growth of these cells on the scaffolds. Moreover, CCK-8 assay showed that the cells proliferate linearly on the 1st, 4th, 7th, and 10th days, but the proliferation activity tended to be maintained on the 14th day (Fig. S1b). The proliferation activity of the BMSCs was higher than that of the two osteocytes on the 4th and 7th days.

The total protein quantitative assay exhibited no significant difference in the total protein content of the cell-derived matrix protein among the groups of BMSCs and osteocytes on and after the 10th day. BMSCs group had more protein on the 4th and 7th days than osteocyte groups probably due to higher cell number in the BMSC groups because BMSCs proliferate faster than osteocytes [50]. All these results suggest that the largest number of cells and proteins could be obtained on the 14th day. Thus, we performed decellularization on the 14th day.

3.2. Preparation of decellularized matrix

3.2.1. Characterization of the DM on 3D-printed PCL scaffolds

Three freeze-thaw cycles and DNase treatment removed all the organelles of BMSCs, WTO, and daCO that grew well for 14 days, full of the surface of the scaffolds as shown in SEM images (Fig. 1c top). After decellularization, the integrity of basement membrane of these cells was all preserved with different morphologies between BMSCs and osteocytes (Fig. 1c middle). Both types of osteocytes and BMSC left cell membrane components, showing dense and clear cell boundaries. OsteocytIC DMs is oval and BMSC-DM is irregular long. The area of a single BMSC-DM was 3–5 times larger than that of osteocytic DM. The surface of BMSC-DM looks smooth, but the osteocytic DM presents a structure of dense honeycomb like network without obvious difference in appearance between the daCO-DM and the WTO-DM. It seemed more daCO than WTO as shown in the 2D cultures in Fig. 1b.

3.2.2. Evaluation of DM components

Ideal decellularization retains as many natural cellular matrix components as possible, such as macromolecular collagen, glycosaminoglycan (GAG), and other biologically active components, while maximizing the removal of immunogenic cellular DNA [63,64]. Hoechst staining showed barely visible DNA in the three DMs of BMSCs and osteocytes (Fig. 1d). DNA quantification showed that residual DNA in the scaffolds was reduced by 95.2%, 95.5%, and 95.2% respectively with no significant difference (n.s.) among these three groups as compared to their original cells before decellularization (Fig. 1e). Collagen were retained by 74.8%, 74.9%, and 74.9% (n.s.) and GAGs retained by 71.9%, 71.9%, and 71.7% (n.s.) (Fig. 1f and g). The efficient decellularization produces three DMs with similar matrix components, that modified 3D-printed PCL scaffolds as functional modules.

Immunofluorescence (IF) staining for VEGF and NGF showed that red fluorescence (positive for VEGF) and green fluorescence (positive for NGF) expressed in daCO-DM were highest compared to the other three DMs (Fig. S6). And the positive expression was higher in WTO-DM than BMSC-DM. The results indicate that daCO-DM can promote angiogenesis and neurogenesis.

3.3. Biocompatibility of daCO-DM modules ex vivo

Good biocompatibility, including adhesion, spreading, and proliferation of cells, is a necessary condition for the application of daCO-DM. We first evaluated the cell viability of newly-seeded BMSCs growing on the daCO-DM modules using a live-dead cell staining assay. After BMSCs cultured on these three modules for 24 h, these modules were stained by LIVE/DEAD staining mixture and visualized under fluorescence microscope. Fluorescent images showed that the BMSCs survive well on all of three modules (Fig. 2a) at survival rates 90.6%, 90.0%, and 90.4%, respectively. There was no significant difference among these three groups (Fig. 2b).

Cell adhesion and spreading were assessed by F-actin cytoskeleton staining. Rhodamine phalloidin has a high affinity with F-actin microfilaments and can display focal adhesion [50]. As shown in Fig. 2c, the newly inoculated BMSCs adhered well and spread more in the three DM modules as compared to none-DM. Where, the daCO-DM induced largest spreading of the BMSCs, followed by the WTO-DM; the BMSC-DM is less, and the none-DM is the least (Fig. 2d). Moreover, as rhodamine phalloidin stains stress fibers, there was more and longer F-actin stress fibers in osteocytic DM modules than in the none-DM and BMSC-DM ones. Moreover, the daCO-DM induced stress fiber is the longest, while the none-DM is smallest and shortest. Therefore, daCO-DM is most conducive to the generation and arrangement of F-actin stress fibers, resulting in full expansion and strong adhesion of cells.

The longest stress fiber could promote osteoblast differentiation of the BMSCs. To explore the role of actin cytoskeleton in osteogenic differentiation, cytoskeleton depolymerization was induced by CytoD [51]. After BMSCs were cultured in daCO-DM modified scaffold with Cyto D treatment, F-actin staining showed that the cytoskeleton was completely destroyed, while the cells in the group without Cyto D spread well (Fig. 2f). AP staining showed that Cyto D treatment significantly reduced AP activity (Fig. 2g). qPCR results showed that Cyto D significantly reduced the expression of osteoblast marker genes (Fig. 2h).

BMSC proliferation on the modules in each group was detected by CCK-8 kit. The results showed that the cells proliferated with the culture time in all of the four types of modules (Fig. 2e), and DM modules caused higher proliferation activity than none-DM modules. Although the cell proliferation in daCO-DM modules was slightly higher but did not reach significant difference than in WTO-DM and BMSC-DM groups, suggesting that DM could promote the proliferation activity of BMSCs.

The above results show that DM-modified 3D printed-PCL scaffolds have good biocompatibility in adhesion, spreading, and proliferation of cells. Subsequently, we evaluated its osteogenic ability.

3.4. daCO-DM promotes osteoblast differentiation and mineralization ex vivo

3.4.1. AP staining and quantitative AP biochemical activity assay

To compare the effects of daCO-DM, WTO-DM, and BMSC-DM on the

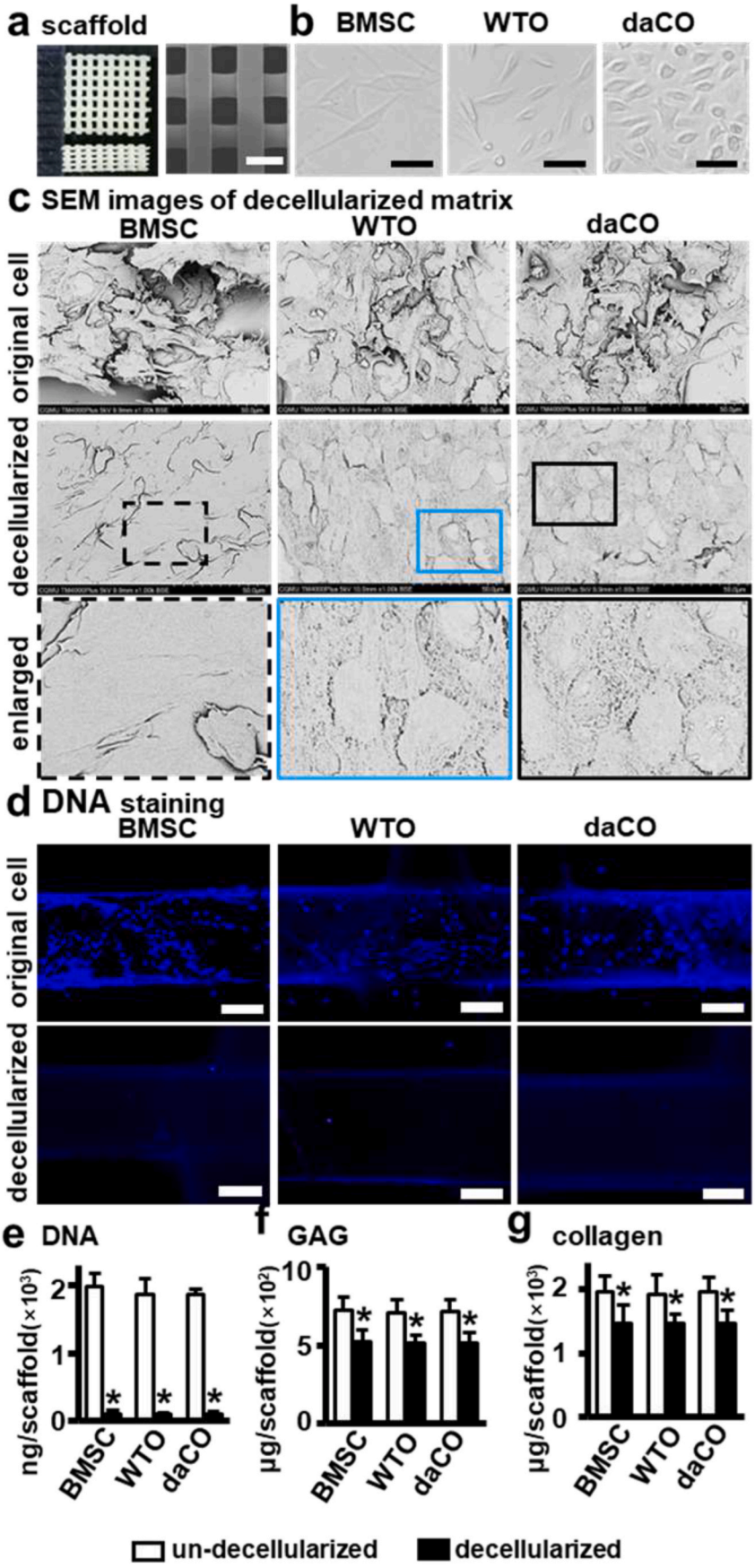

Fig. 1. Preparation of DM modified 3D printed PCL scaffold. (a)3D printed PCL scaffold. Scale bar 500 μm. (b) Isolated BMSCs and osteocytes growing on dish. Scale bar 20 μm. (c)SEM images of scaffolds un-decellularized and decellularized. Scale bar 50 μm. (d) Hochest 33258 staining for cell nucleus before and after un-decellularized and decellularized. Scale bar 100 μm. (e–g) DNA, collagen, and GAGs quantitation of the scaffolds un-decellularized and decellularized. BMSC, bone marrow stromal cell; WTO, wild-type osteocyte; daCO, osteocyte with dominant active β-catenin. Images and data are representative of n = 3 individual experiments. Data were expressed as mean ± SD. $*p < 0.05$ v.s. un-decellularized by one way ANOVA.

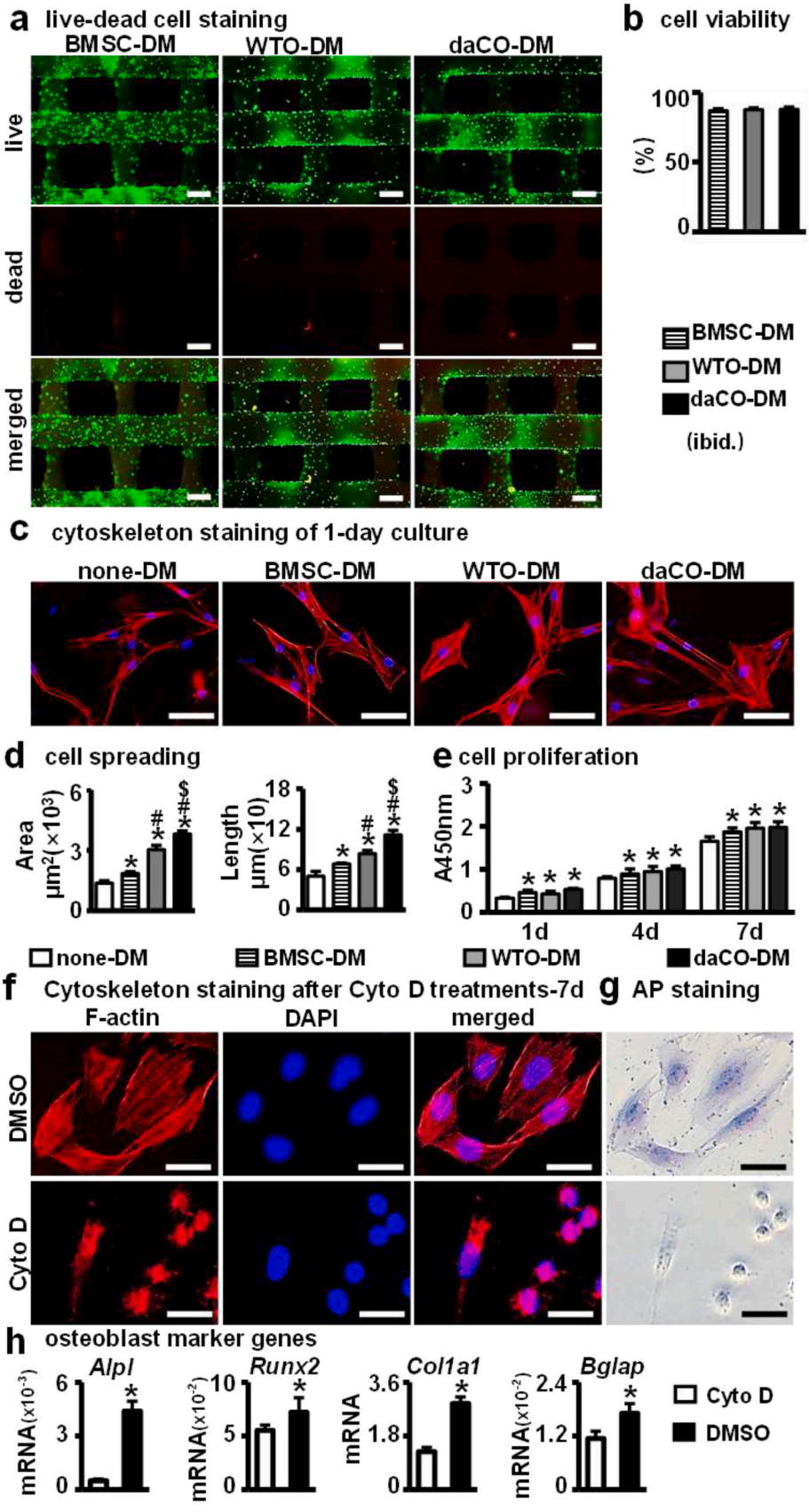

Fig. 2. Biocompatibility assay of DM modified 3D printed PCL modules. (a) Live-Dead staining to analyze the viability of BMSCs on DM modified modules for 24 h, live cells (green) and dead cells (red). Scale bar 250 μm. (b) ImageJ analysis of the vitality of BMSCs on DM modified modules. (c) Cytoskeleton staining of BMSCs cultured on DM modified modules and none-DM scaffolds after 24 h. Scale bar 50 μm. (d) ImageJ analysis of cell speading area. (e) CCK-8 analysis the proliferation of cells on DM modified modules and none-DM scaffolds on day 1,4,7. (f) Cytoskeleton staining and (g) AP staining of BMSCs cultured on four groups scaffolds with/without Cyto D. (h) Gene expressions of *Alpl, Runx2, Col1a1,* and *Bglap* after 7 days of culture. DM, decellularized matrix; none-DM, PCL; BMSC, bone marrow stromal cells; WTO, wild-type osteocytes; daCO, osteocyte with dominant active β-catenin. Images and data are representative of n = 3 individual experiments. Data were expressed as mean ± SD. $^{*}p < 0.05$ v.s. none-DM; $^{\#}p < 0.05$ v.s. BMSC-DM, $^{\$}p < 0.05$ v.s. WTO-DM by one way ANOVA. Multiple influencing factors analysis by two way ANOVA.

osteoblast differentiation of BMSCs, the new batch BMSCs from C57BL/6 mice were harvested and seeded on these three DM-modified modules. After cultured for 7 and 14 days, AP staining of these modules showed that the 14-day cultures of the 3 groups displayed higher AP activities than 7-day cultures, correspondingly. At both times, the daCO-DM group had the strongest positive AP staining (Fig. 3a). In addition, there was no obvious difference between the WTO-DM and BMSC-DM groups in 7-day cultures.

The results of quantitative AP biochemical assay were consistent with that of AP staining (Fig. 3b). At 7 days, the AP activity in the daCO-DM group was 2.2 times that of the WTO-DM group, and 2.0 times that of the BMSC-DM group. There was no significant difference between the two groups. At 14 days, AP activity in the daCO-DM group was 1.7 times that of the WTO-DM group and 2.1 times that of the BMSC-DM group. WTO-DM group was 1.2 times that of the BMSC-DM group.

These results showed that osteocytic DM has strongest ability in osteoblast differentiation than BMSC-DM, and that the osteoblast differentiation with the daCO-DM is much higher than that with the other two DMs, proving that the daCO-DM could provide most suitable microenvironment for the osteogenic differentiation of BMSCs.

3.4.2. Effects of daCO-DM on the expression of osteoblast marker genes ex vivo

qPCR measured the mRNA level of osteoblast marker genes, including *Alpl*, *Col1a1*, *Bglap*, and *Runx2* in the new batch of primary BMSCs growing in these 3 types of DM-modified modules for 7 and 14 days, respectively. The results showed that the daCO-DM robust enhanced the expression of these 4 genes in both 7- and 14-day cultures (Fig. 3c) compared to the other 2 DM groups. WTO-DM also enhanced osteoblast differentiation compared to BMSC-DM as well. These data demonstrate that osteocytes are a good cell source of DM to promote the differentiation of BMSCs into osteoblasts; in particular, daCO-DM is a potent osteogenic niche.

3.4.3. Effects of daCO-DM on mineralization ex vivo

Mineralization is the last step in bone formation. To further evaluate the effect of these 3 types of DMs on the mineralization of BMSCs, the new batch of BMSCs from C57BL/6 mice were seeded on these 3 DM modules and grew in growth medium for the first 7 days, and then cultured in osteogenic medium for another 14 days. The mineralization was measured by bone noddle formation assay with alizarin red S staining. The results show that the mineralization induced by daCO-DM is the strongest, that induced by WTO-DM is smaller, and that induced by BMSC-DM is the least (Fig. 3d). The quantitative analysis confirmed the staining results. DaCO-DM induced mineralization was 1.6- and 2.2-fold higher than WTO-DM and BMSC-DM respectively, and WTO-DM induced one was 1.3-fold stronger than BMSC-DM (Fig. 3e). These results suggested that daCO-DM has better mineralization ability than WTO-DM and BMSC-DM ex vivo.

3.5. Bone formation by daCO-DM in vivo

To evaluate the bone repair function of daCO-DM, a critical-sized (≥4.0 mm in diameter) parietal bone defect model was established in C57BL/6 mice [54]. daCO-DM modules and its controls WTO-DM, BMSC-DM, or none-DM were cut to 4.5 mm circular scaffold in diameter (Fig. 4a) to be implanted into the defects (Fig. 4b). At 4- and 8-weeks after implantation, cellular and molecular base of bone repair were evaluated. Gross observations of the grafts implanted in vivo at 4 weeks and 8 weeks exhibited more bone regenerated in daCO-DM mudule than the controls (Fig. 4c).

3.5.1. PET-CT assessment of daCO-DM on new bone formation

PET-CT was used to detect in situ new bone at the bone defects. Four weeks after implantation, the three DM modules formed bone; however, there is little bone formed with the none-DM modules (Fig. 4d left). ImageJ analysis of newly formed bone showed that the BA/TA of daCO-DM group accounted for 39.0% the defect area (tissue area), which was significantly higher than the other three groups, i.e. none-DM (9.0%), BMSC-DM (14.0%), and WTO-DM groups (27.0%) (Fig. 4f). At 8 weeks, the BA/TA of each group was higher than the counterparts at 4 weeks. In particular, the BA/TA of daCO-DM group was 60.0%, which was 3.5-, 2.9-, and 1.5-fold of the other three groups (17.0%, 21.0%, and 34.0%) (Fig. 4f).

PET-CT data displayed that daCO-DM greatly accelerates the repair of critical-sized bone defects compared to WTO-DM and BMSC-DM, especially compared to none-DM.

3.5.2. Bone histomorphometry on daCO-DM formed bone

HE staining of bone sections showed that daCO-DM module formed most of the bone, and the BV/TV was 16.3% at 4 weeks, which was higher than that of the other three groups (0.4%,1.34%, and 5.7%) (Figs. S2a and b), but the tissue formed in the pure PCL group (none-DM) does not look like bone.

At 8 weeks, the daCO-DM group also had most new bone formed in the modules and well-integrated with the parietal bone of mice (Fig. 4c–e). In addition, the new bone had the morphological characteristics of natural bone tissue with a concentrated structure, contains osteocytes embedded in the mineralized matrix, and osteoblasts were arranged at the outer edge of the new bone (Fig. 4e enlarged image). However, the new bone formed in the other 3 groups did not have dense structure, which was different from that in the daCO-DM group. In addition, the BV/TV formed in daCO-DM module was the highest, 54.1%, which was 3.9-, 3.2-, and 1.8-fold of that formed in the other three modules (14.3%,17.3%, and 31.0%) (Fig. 4g).

In addition, the bone volume was parallel to the number of osteoblasts. The number osteoblast per bone area (N.Ob/B.Ar) was the highest in the newly formed bone of daCO-DM groups ($3.2 \times 10^2/mm^2$), which was 3.3-, 2.9-, 1.7-fold of the other three groups (1.0, 1.1, and $1.8 \times 10^2/mm^2$) (Fig. 4g).

The results clearly show that the bone regeneration ability of osteocytic DM is stronger than that of BMSC-DM, and daCO-DM is much higher than WTO-DM, indicating that the daCO-DM is an effective DM to recruit cells for bone regeneration and repair in vivo.

3.6. Osteoblast activity in daCO-DM-induced bone

Bone is formed by mineralization of collagen secreted by osteoblasts. Type I collagen is the main component of bone organic matrix. After Picrosirius red staining, type I collagen was red under light microscope; while, under the polarized light microscope, it was yellow to orange, in the shape of fiber bundle, and has strong double refraction of red and yellow/orange [65]. At 4 weeks, there were more collagen fibers in daCO-DM group, which were arranged neatly and closely, followed by WTO-DM group. There were few collagen fibers in BMSC-DM group, which were arranged loosely and disorderly. And there was almost no collagen in none-DM group (Fig. 5a).

At 8 weeks, more collagen was formed in all groups compared with that at 4 weeks. DaCO-DM group generated red dense collagen under light microscope, and strong double refraction of red and yellow under polarized light microscope, which is similar to natural bone tissue [57] (Fig. 5b). The collagen production in WTO-DM group was the second, and it was the least in BMSC-DM group and none-DM group. Especially in the none-DM group, the arrangement of collagen fibers was disordered. Therefore, osteocytic DMs induced osteoblast can significantly promote the formation of type I collagen in vivo than BMSC-DM induced ones. Therefore, the osteogenic ability of osteoblasts induced by osteocytic DM is stronger than that of BMSC-DM. Obviously, the function of daCO-DM is much higher than that of WTO-DM.

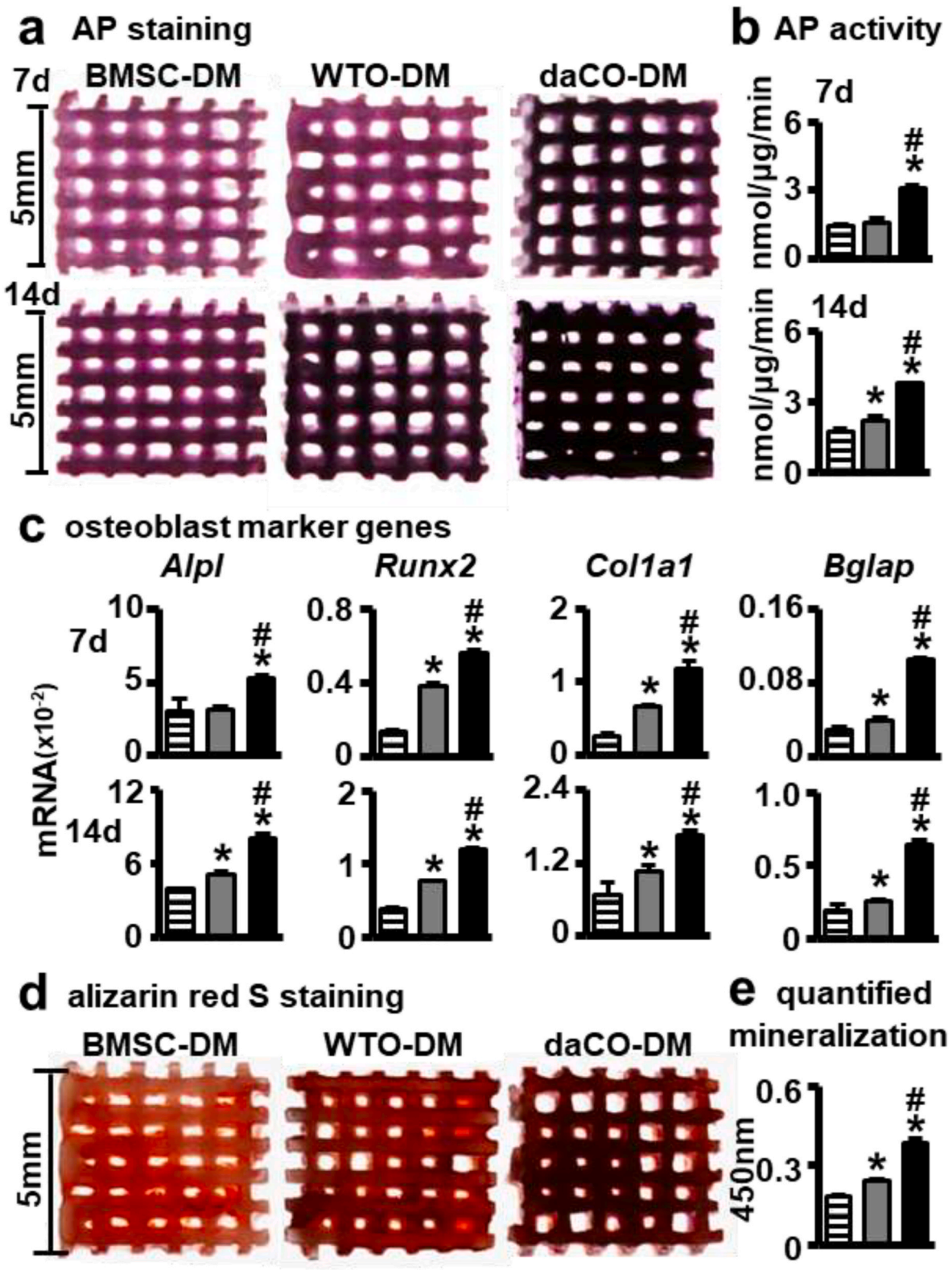

Fig. 3. daCO-DM modified 3D-printed modules promoted BMSCs osteoblast differentiation and mineralization. (a,b) AP staining and AP biochemical activity assays of BMSCs on DM-modified modules after culturing in basal medium for 7 and 14 days, respectively. (c) Gene expressions of *Alpl, Runx2, Col1a1,* and *Bglap* after 7 and 14 days of culture, respectively. (d) Alizarin red S stained calcium mineral nodules deposited by BMSCs on BMSC-DM, WTO-DM and daCO-DM modified modules for 14 days culture in osteogenesis induction medium respectively. (e) Mineralization quantification were measured at day 21. DM, decellularized matrix; BMSC, bone marrow stromal cell; WTO, wild-type osteocyte; daCO, osteocyte with dominant active β-catenin. Images and data are representative of n = 3 individual experiments. Data were expressed as mean ± SD. $^{*}p < 0.05$ v.s. BMSC-DM, $^{\#}p < 0.05$ v.s. WTO-DM by one way ANOVA.

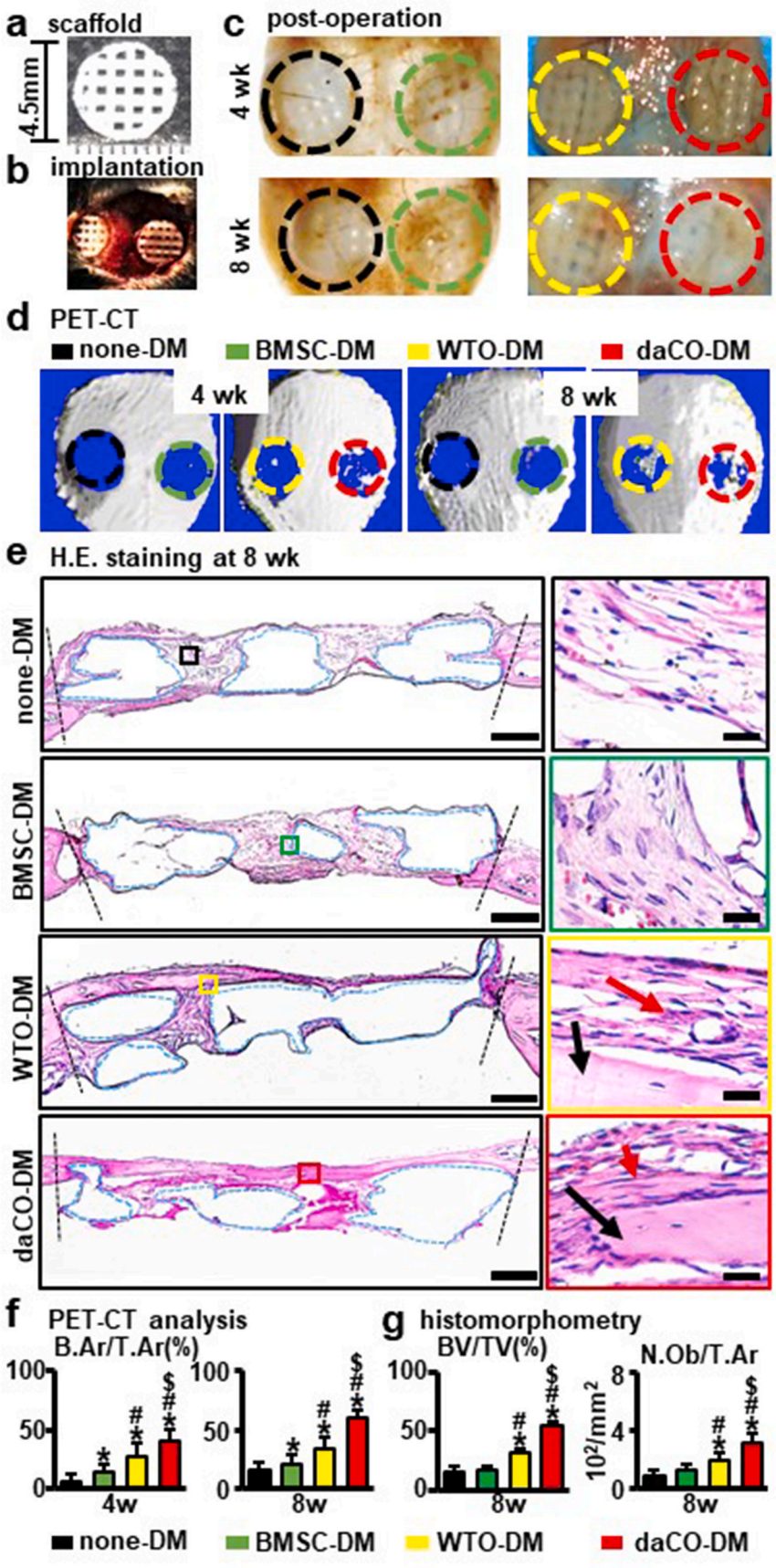

Fig. 4. Effect of daCO-DM modified 3D-printed module on bone regeneration. (a) Circle implanted module (Φ = 4.5 mm) before implantation. (b) Critical-sized parietal bone defect model. (c) Modules were implanted in vivo for 4weeks and 8 weeks (before harvest). (d) PET-CT images of mouse critical parietal bone defect implanted with four group modules of none-DM, BMSC-DM, WTO-DM, and daCO-DMat 4 and 8 weeks, n=5. (e) H.E. staining of the cross-sections to show the histological morphology of the regenerative repair at 8 weeks. red arrow, osteoblast; black arrow, new bone. Scale bars 500 μm and 20 μm.(f) The relative new bone formation was calculated by normalization to new bone formation area in the defects, which was measured by ImageJ software. Bone area per tissue area (B.Ar/T.Ar). (g) Bone formation ratio was measured by ImageJ software based on H.E. stained cross-sections at 8 weeks BV/TV, bone volume per tissue volume, N.Ob/T.Ar, number of osteoblasts per tissue area , n = 5. DM, decellularized matrix; none-DM, PCL scaffold; BMSC, bone marrow stromal cell; WTO, wild-type osteocytes; daCO, osteocyte with dominant active β-catenin. Sections with newly formed bone were measured for each mouse. Data were expressed as mean ± SD. $^{*}p < 0.05$ v.s. none-DM $^{\#}p < 0.05$ v.s. BMSC-DM, $^{\$}p < 0.05$ v.s. WTO-DM by one way ANOVA.

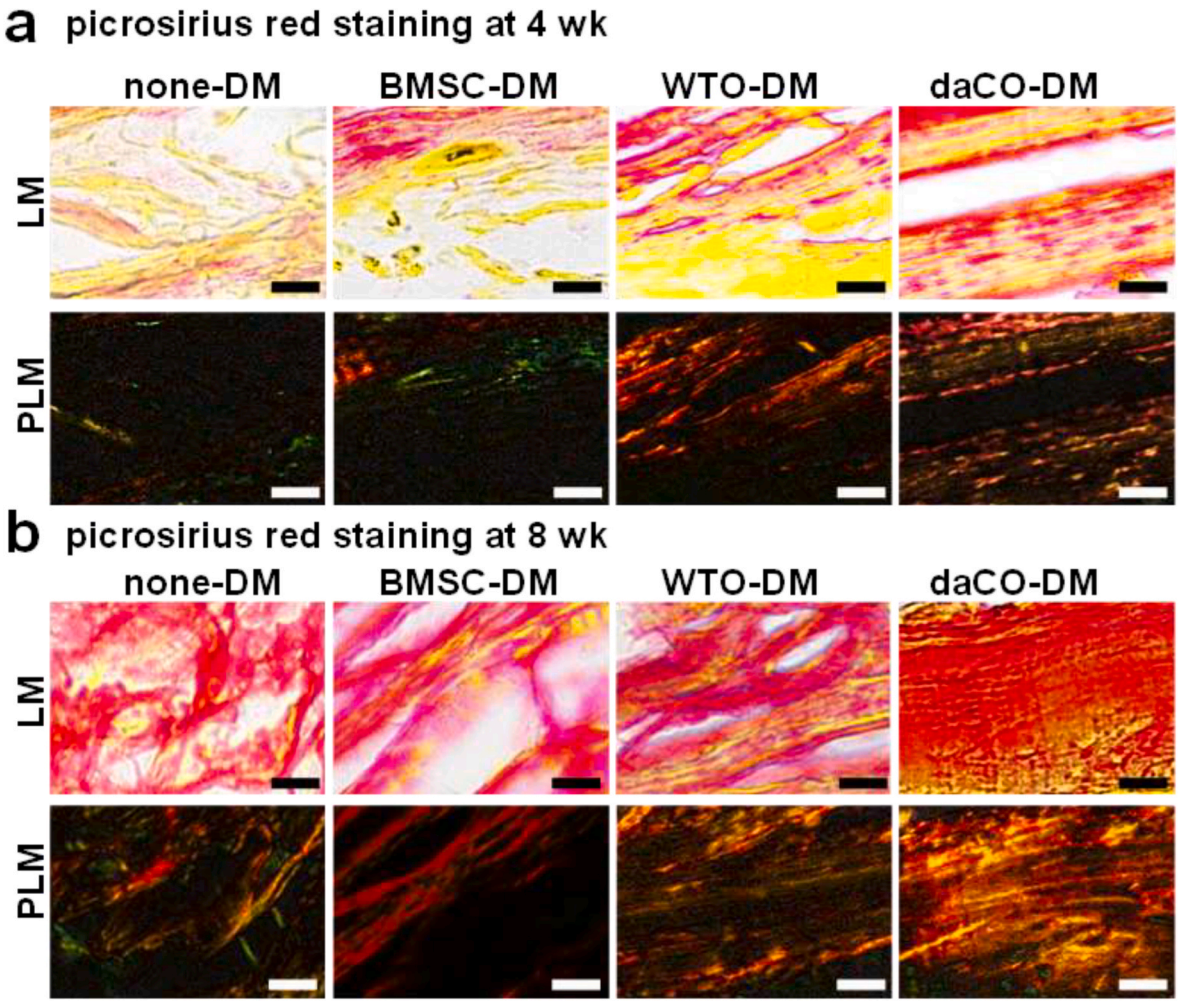

Fig. 5. Osteoblast activity in daCO-DM-induced bone. After implantation 4 wk (a) and 8 wk (b), picrosirius red staining showed type I collagen was bright red or yellow under light microscope (LM) and yellow or red, closely arranged and strong birefringence under polarized light microscope (PLM). Scale bar 50 μm. Sections with newly formed bone were measured for each mouse and 5 mice were analyzed for each group. DM, decellularized matrix; none-DM, PCL scaffold; BMSC, bone marrow stromal cell; WTO, wild-type osteocytes; daCO, osteocyte with dominant active β-catenin.

3.7. Osteoclastogenesis by daCO-DM

Bone resorption is the process of osteoclasts decomposing and absorbing bone matrix, which plays an important role in bone reconstruction [66]. TRAP staining of tissue sections showed that at 4 weeks after implantation, Oc.S/T.Ar of daCO-DM was 10.0 μm/mm^2, 2.3-fold of WTO-DM, while osteoclasts were hardly observed in BMSC-DM and none-DM groups (Fig. 6a, c). At 8 weeks, BMSC-DM group and none-DM group finally formed a small number of osteoclasts, and Oc.S/T.Ar about 5.6 μm/mm^2 (n.s.). The Oc.S/T.Ar almost doubled in the daCO-DM (20.3 μm/mm^2) and WTO-DM (14 μm/mm^2) groups compared with that at 4 weeks (Fig. 6b and c). Since we observed that the osteoclasts grew in the newly formed bones and were interconnected with each other, their number is calculated based on Oc.S/T.Ar.

To compare the effects of daCO-DM, WTO-DM, BMSC-DM, and none-DM on osteoclastogenesis, the BMMs were cultured on these 4 types of modules. 5 days later, TRAP staining results showed that daCO-DM induced multinucleated osteoclasts as shown in purple red by TRAP staining. Additionally, WTO-DM also induced TRAP-positive cells in its modules; however, such an induction does not happen in the none-DM and BMSC-DM modules (Fig. 6e).

3.8. Angiogenesis by daCO-DM

Blood vessels play an important role in bone regeneration as well, delivering oxygen nutrients, growth factors, and cells etc. for tissue repair [67]. The enhancement of angiogenesis in both osteocytic DM groups was observed by HE staining of tissue sections. After 8 weeks after implantation, the number of new vessels per tissue area (N.Vessel/T.Ar) was 8.1/mm^2 in daCO-DM group, which was 1.6-, 3.2-, and 3.5-fold of WTO-DM group, BMSC-DM group, and none-DM group (Fig. 7a and b). Immunofluorescence (IF) staining of vascular markers CD31 and Endomucin also confirmed the formation of blood vessels. The results showed that the red fluorescence (positive for CD31) and green fluorescence (positive for Eodomucin) induced by daCO-DM were significantly increased in the newly formed bone compared to that by the other three DMs (Fig. 7d). In addition, qPCR detection found that among the BMSCs growing on these 3 DM modules, the expression of angiogenesis related genes *Vegfa* and *Angpt1* was the highest in the BMSCs growing on daCO-DM modules (Fig. 7c). The evidence indicates that daCO-DM may promote the formation of H-type blood vessels in vivo, so as to ensure the osteogenic function of the module, which is conducive to the regenerative repair of bone defects.

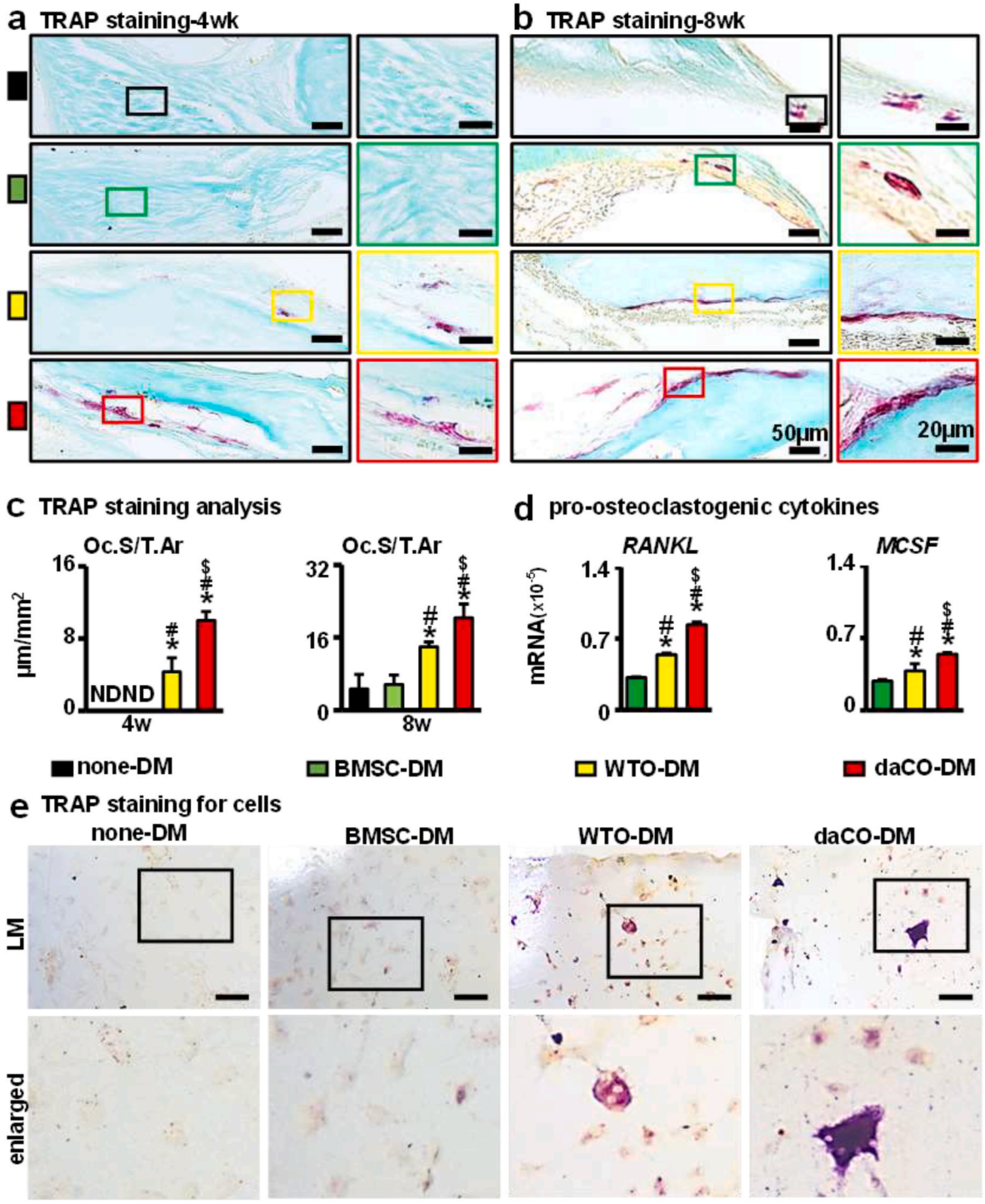

Fig. 6. Effect of daCO-DM modified 3D-printed module on osteoclastogenesis. (a,b) At 4 and 8 weeks, static histological analysis (TRAP staining) on the surface of osteoclasts was performed after the implantation of modules. The red part is osteoclast positive, and the right figure is the enlarged image. Scale bars 50 μm and 20 μm. (c) 4 weeks and 8 weeks quantitative analysis: osteoclast surface per tissue area (Oc.S/T.Ar). (d) Gene expressions of *RANKL* and *MCSF* after 14 days of BMSCs culturing on DM modifed scaffolds ex vivo. (e) TRAP staining for BMMs cultured in DM modified scaffolds. DM, decellularized matrix; none-DM, PCL; BMSC, bone marrow stromal cell; WTO, wild-type osteocytes; daCO, osteocyte with dominant active β-catenin. ND means not detected. Sections with newly formed bone were measured for each mouse and 5 mice were analyzed for each group. Data were expressed as mean ± SD. $^{*}p < 0.05$ v.s. none-DM; $^{\#}p < 0.05$ v.s. BMSC-DM, $^{\$}p < 0.05$ v.s. WTO-DM by one way ANOVA.

3.9. Neurogenesis by daCO-DM

Nerve fibers also play an important role in bone formation. Insufficient innervation in the bone defect area may delay bone regeneration [59]. IF was used to evaluate the expression of neural markers β3-Tubulin and NeuN in the implanted modules after 8 weeks to detect neurogenesis in vivo. The expression of these two neural genes was much higher in the daCO-DM-induced bone than in the other three DM module-generated bone (Fig. 8a). Especially in none-DM and BMSC-DM implants, the expression level is lower and lowest. qPCR detection found

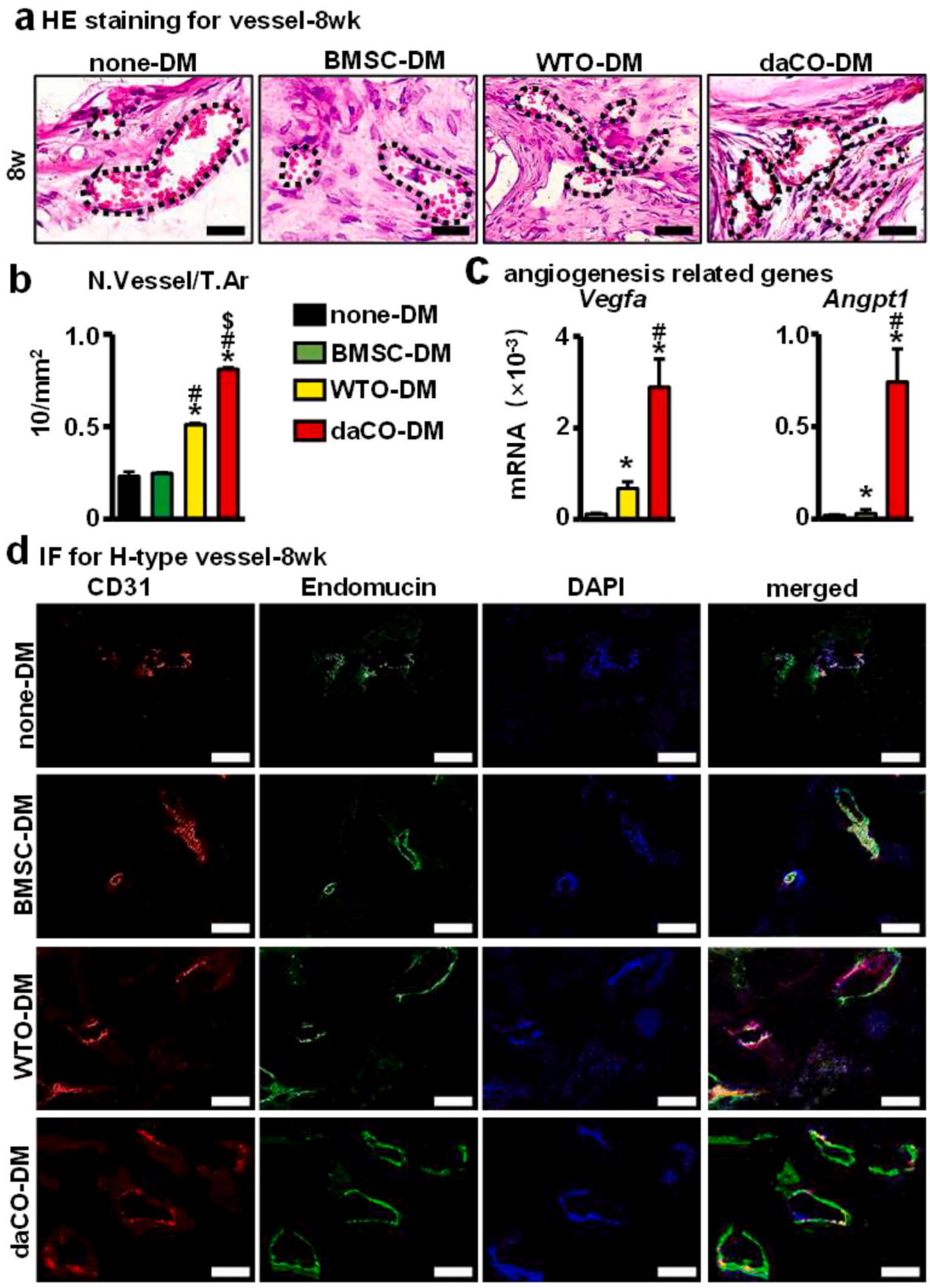

Fig. 7. Angiogenesis of daCO-DM modified 3D-printed module. (a) At 8-week, HE staining to analyze the morphology of blood vessels in four groups. Scale bar 20 μm. (b) Semi-quantitative analysis of blood vessels. number of blood vessels per tissue area (N.Vessel/T.Ar). (c) Gene expressions of *Vegfa* and *Angpt1* after 14 days of BMSCs culturing on DM modifed scaffolds. (d) Immunofluorescence of CD31 and Endomucin showed H-type angiogenesis in vivo. Scale bar 20 μm. DM, decellularized matrix; none-DM, PCL; BMSC, bone marrow stromal cell; WTO, wild-type osteocytes; daCO, osteocyte with dominant active β-catenin. Sections with newly formed bone were measured for each mouse and 5 mice were analyzed for each group. Data were expressed as mean ± SD. $^{*}p < 0.05$ v.s. none-DM; $^{\#}p < 0.05$ v.s. BMSC-DM, $^{\$}p < 0.05$ v.s. WTO-DM by one way ANOVA.

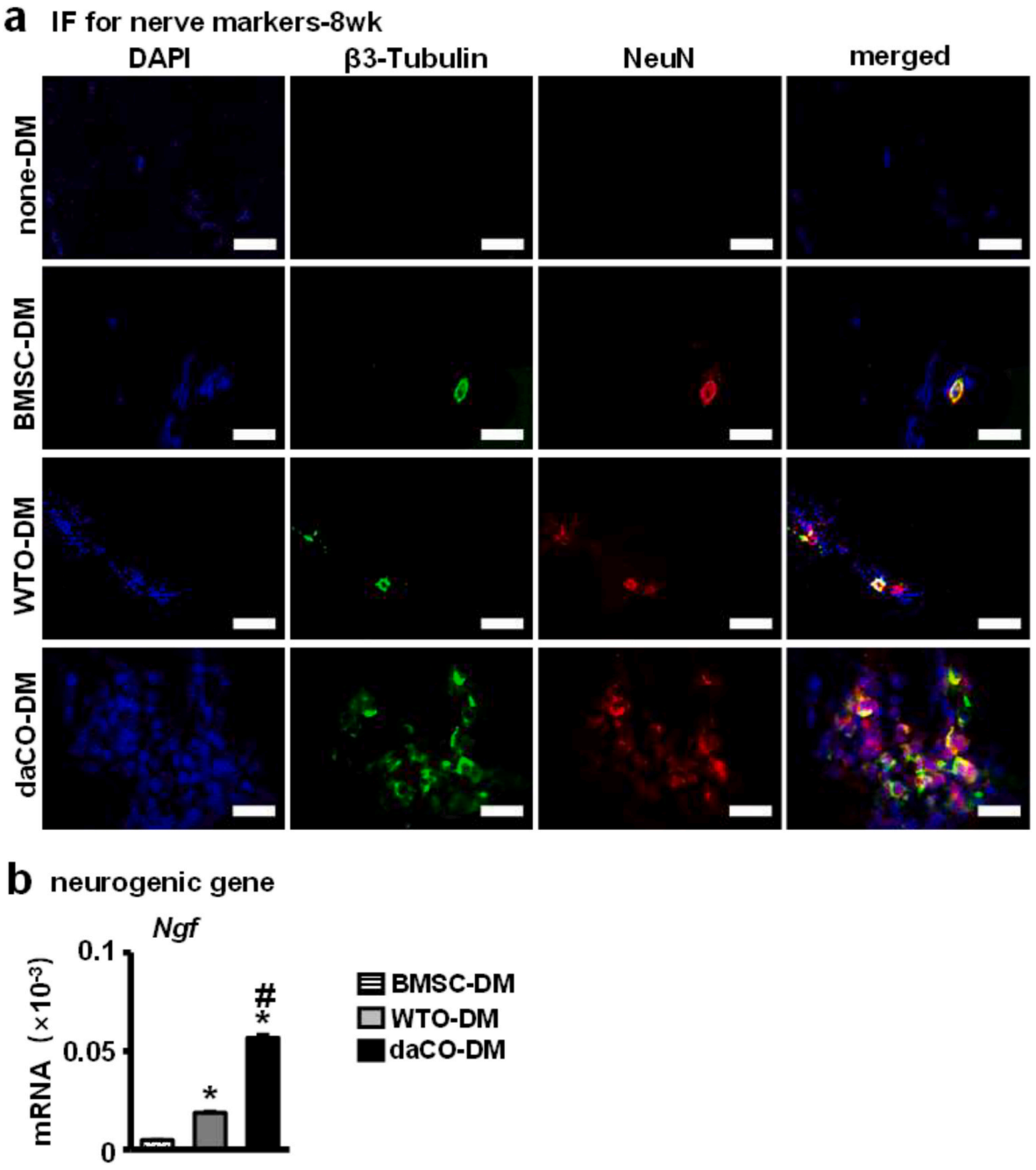

Fig. 8. Effect of daCO-DM modified 3D-printed module on neurogenesis. (a)Immunofluorescence of β3-Tubulin and NeuN showed nerve in vivo. Scale bar 20 μm. (b)Gene expressions of *Ngf* after 14 days of BMSCs culturing on DM modifed scaffolds. DM, decellularized matrix; none-DM, PCL; BMSC, bone marrow stromal cell; WTO, wild-type osteocytes; daCO, osteocyte with dominant active β-catenin. Sections with newly formed bone were measured for each mouse and 5 mice were analyzed for each group. Data were expressed as mean ± SD. $^{*}p < 0.05$ v.s. none-DM; $^{\#}p < 0.05$ v.s. BMSC-DM, $^{\$}p < 0.05$ v.s. WTO-DM by one way ANOVA.

that among the BMSCs growing in DM modules, the expression of neurogenesis related genes *Ngf* was the highest in daCO-DM modules (Fig. 8d). These results suggest that daCO-DM promotes neurogenesis in vivo.

4. Discussion

To select a functional cell source for decellularized matrix, we compared 3 cell types, primary osteocytes with/without dominant active Wnt/β-catenin signaling and primary BMSCs. Decellularization removes all organelles and most DNA, and retains a large amount of collagen and GAG. daCO-DM produces more and longer stress fibers, conducive to cell adhesion, spreading, and osteogenesis. In vivo, daCO-DM produces neatly arranged and dense type-I collagen, which is similar to and integrated well with the host bone, whereas the other 3 DMs do not have this ability. BV/TV and osteoblast number were much higher than the other three DMs. daCO-DM induces more osteoclasts than WTO-DM, but neither BMSC-DM nor none-DM shows this induction. daCO-DM promotes the expression of *RANKL* and *MCSF*, *Vegfa* and *Angpt1*, and nerve growth factor *Ngf* for osteoclast differentiation, vascularization, and neurogenesis. daCO-DM produces more H-type blood vessels and expresion of nerve cell markers β3-tubulin and NeuN. daCO-DM, a new bioactive material based on multifunctional daCO, realizes bone regeneration with metabolic activity and

neurovascularization, restores blood supply to the defect area, activates bone remodeling to accelerate the repair of bone fefects, which is expected to be transformed into clinical application.

Cell-derived decellularized matrix has been widely used in bone tissue engineering [68,69]. However, as far as we know, DM has not been reported to have the same four functions as daCO-DM does in the formation of osteoblasts, osteoclasts, blood vessels, and nerves. Currently, most of the cell-derived DM have osteogenic properties, such as human fetal MSC [70], hMSC [71], mouse MC3T3-E1 [72], human osteoblast line MG63 [73]. In addition, DMs from the co-culture of hMSC and human umbilical vein endothelial cells (HUVEC) [74] or MC3T3-E1 and fibroblast NIH/3T3 [75] have dual functions of osteogenesis and angiogenesis. The formed blood vessel will provide nutrients, growth factors, and cells, necessary for the regenerated bone, in addition and will excrete metabolites as well. Moreover, DM of mouse osteocytic cell line MLO-5A [25] can also promote both osteogenesis and angiogenesis. In these mentioned cases, the DMs from co-culture of MC3T3-E1 and NIH/3T3 [75], MG63 [73], and MC3T3-E1 [76] have been demonstrated to repair critical-sized bone defect in mice, rats, and rabbits, respectively. In summary, the selection of cell types is of great significance to the function of DM. None of the DMs from the above cell types reported the production of osteoclasts or the expression of nerve markers.

Osteoclasts play an important role in bone development [77]. Our previous study found that osteocytic Wnt mediates anabolic and catabolic actions in mice [35], suggesting a participation of osteoclasts in bone formation. Osteoclasts not only control bone remodeling [78,79], but also recruit stem cells for osteoblast differentiation by producing active transforming growth factor-β (TGFβ1) from bone matrix [66], and promote H-type angiogenesis [80–82]. In the process of osteoclast bone resorption, transforming growth factor-β (TGF-β) and insulin-like growth factor 1 (IGF-1) are released from bone matrix to induce mesenchymal stem cells (MSCs) to migrate and differentiate into osteoblasts to form new bone [83,84]. It has also been reported that osteoclasts secrete PDGF-BB to induce MSCs or osteoblasts migration [85,86]. During bone remodeling, pre-osteoclasts secrete PDGF-BB to induce angiogenesis, and sufficient blood supply transports nutrients, oxygen, minerals, and metabolic wastes necessary to maintain osteoblast bone matrix synthesis and mineralization [87], thus inducing appropriate osteogenesis. In this study, qPCR results showed that after 14 days of culture, osteocytic DM induces BMSCs to express pre-osteoclastic cytokines *RANKL* and *MCSF*, in which daCO-DM group displays significantly higher expression than WTO-DM. In vivo, 4 weeks after DM module implantation, osteoclasts were observed only in osteocytic DM groups, in which Oc.S/T.Ar of daCO-DM group is 2.3 times of that in WTO-DM group, whereas osteoclasts were not observed in BMSC-DM group and none-DM group. This study shows that in the early stage of osteogenesis, osteocytic DM promotes the formation of osteoclasts, so as to play the role of bone resorption in bone development, restore blood supply in the defect area, promote osteogenic differentiation of stem cells and expression of neural markers, and achieve rapid repair effect. 8 weeks after implantation, daCO-DM group was still the highest in Oc.S/T.Ar, which was 1.5, 3.6, and 3.9 times of that in the other three groups, respectively. A small number of osteoclasts were also generated in BMSC-DM and none-DM groups. This may be due to the coupling effect of bone formation and bone resorption.

The method of decellularization also has effects on the composition and microstructure of DM [88]. It is very important to find effective way to remove organelles and cellular DNA that cause inflammatory response, while maintaining the high integrity of the composition and structure of the cell matrix [89]. At present, the cell-derived DM decellularization treatments mainly include physical, chemical, and biological methods. Boram et al. found no significant difference in DNA removal by either three freeze-thaw cycles (F/T) or sodium dodecyl sulfate (SDS) in hypoosmotic solution, however, F/T retains 75.64% GAGs, much higher than 33.28% by SDS [14]. SDS in decellularization is too intense to retain cell matrix components. Li et al. found that F/T plus Triton-X100 treatment is the most effective method to remove DNA and retain the structure and collagen, and the decellularized matrix is conducive to the proliferation and osteogenic differentiation of BMSCs [90]. Aldemir Dikici et al. found that more than 95% DNA is removed by three F/T combined with DNase enzyme treatment, while only 75% DNA was removed by three F/T, and DNA enzyme had no effect on the content of matrix components (collagen and deposited calcium) [25]. Moreover, the damage of matrix structure was the least by F/T [91,92]. Based on the above studies, we selected the last decellularization treatments of three F/T combined with DNase, which retains 71% GAGs and 74% collagen and effectively removes DNA by 95% (Fig. 1e–g).

In vitro F-actin cytoskeleton staining, daCO-DM group promoted the adhesion of BMSCs and the formation of F-actin stress fibers (Fig. 2c), thus promoting osteogenic differentiation [50,93]. SEM showed that the DM of BMSC was smoother than that of osteocytes, and the two kinds of osteocyte had the same honeycomb like network structure. The difference in the structure of DMs is caused by different cell types. The primary daCO is oval and fat (Fig. 1b), while WTO looks thinner, and the osteocytes are smaller than BMSCs. Although DM in all three groups promoted cell adhesion and proliferation with no significant differences since collagen and GAGs content among the three groups are the same. Although DM has been extensively studied by researchers, the mechanism by which DM derived from cells induces specific cellular behavior remains unclear [94], and the components of daCO-DM promoting osteogenesis remain to be revealed.

As for the promotion of neurogenesis by osteocytes, there is still no direct evidence. Even though, osteocytes express NGF [95], which has long occupied a critical role in developmental and adult neurobiology for its many important regulatory functions on the survival, growth, and differentiation of nerve cells in the peripheral and central nervous system [96,97]. This is very meaningful to the brain. daCO-DM may promote neurogenesis, possibly because it may retain the products of Wnt signaling in osteocytes, thus promoting neurogenesis [98], but the specific components need to be further studied.

The daCO-DM modified 3D-printed module developed in this study has good in situ bone regeneration and repair ability. It has good biocompatibility, including cell adhesion, spreading, proliferation, osteogenic differentiation, and mineralization. In vivo, it recruits cells to reach the defect site and produces osteogenic differentiation, osteoclast formation, vascularization, and expression of nerve cell markers. Because organoid is defined by a 3D cell systems that are formed through cell differentiation and self-organization of pluripotent stem cells or tissue-derived progenitor cells, also contains supporting stromal elements [40], daCO-DM module formed organoid bone in vivo. In further study, we will extract osteocytes from patients or from porcine which is the most likely source of xenotransplantation products for humans [99] and activate them with Wnt signaling pathway. Based on osteogenic microenvironment of daCO, we will develop bone regeneration agents, biological ink and other easy-to-use products which can quickly repair bone defects. These materials can also be used for surface coating treatment of scaffolds or implants to enhance interface integration and prolong the service life of implants, so as to provide new ideas for the research and development of bone repair materials and promote clinical transformation and application.

5. Conclusions

In this study, based on the osteocytes with activation of Wnt signaling (daCO) osteogenic microenvironment, a daCO-DM modified 3D printing PCL module was constructed by F/T combined with DNase treatment of the daCO. The daCO-DM has good biocompatibility, promotes osteogenic differentiation and mineralization in vitro, and induces bone regeneration in vivo, including the formation of osteoblasts, osteoclasts, and H-type blood vessels, and nerve-like cells expressing nerve markers, and accelerates the repair of critical-sized bone defects in

mice. The daCO forms multifunctional organoid bone, which is conducive to clinical transformation application, and breaks through the bottleneck of low bioactivity and difficult shape matching of bone repair materials in the market.

Funding

This research was funded by the National Natural Science Foundation of China U1601220 (X.T.),81672118 (X.T.), 82072450 (X.T.), 82002310 (Y.M.), Chongqing Science and Technology Commission—Basic Science and Frontier Technology Key Project cstc2015jcyjBX0119 (X.T.), and CQMU Program for Youth Innovation in Future Medicine, W0075 (Y.M.).

Declaration of competing interest

The authors declare that they have no competing financial interests or personal relationships that could have appeared influence the work reported in the paper.

CRediT authorship contribution statement

Xiaofang Wang: Methodology, Formal analysis, Investigation, Resources, Data curation, Writing – original draft. **Yufei Ma:** Conceptualization, Methodology, Validation, Data curation, Investigation, Formal analysis, Writing – original draft. **Jie Chen:** Methodology, Software, Formal analysis, Investigation, Writing – original draft. **Yujiao Liu:** Writing – original draft, Methodology, Formal analysis, Investigation, Resources. **Guangliang Liu:** Methodology, Investigation. **Pengtao Wang:** Validation, Resources, Writing – original draft. **Bo Wang:** Methodology, Resources. **Makoto M. Taketo:** Resources. **Teresita Bellido:** Resources. **Xiaolin Tu:** Conceptualization, Methodology, Validation, Data curation, Resources, Writing – original draft.

Declaration of competing interest

We declare that we have no financial and personal relationships with other people or organizations that can inappropriately influence our work, there is no professional or other personal interest of any nature or kind in any product, service and/or company that could be construed as influencing the position presented in, or the review of, the manuscript entitled.

Appendix A. Supplementary data

Supplementary data to this article can be found online at https://doi.org/10.1016/j.bioactmat.2022.07.017.

References

[1] R. Li, H. Wang, J.V. John, H. Song, M.J. Teusink, J. Xie, 3D hybrid nanofiber aerogels combining with nanoparticles made of a biocleavable and targeting polycation and MiR-26a for bone repair, Adv. Funct. Mater. 30 (49) (2020).
[2] C. Myeroff, M. Archdeacon, Autogenous bone graft: donor sites and techniques, J. Bone Joint Surg. Am. 93 (23) (2011) 2227–2236.
[3] J.L.Y. Peng, H. Lin, S. Tian, S. Liu, F. Pu, L. Zhao, K. Ma, X. Qing, Z. Shao, Endogenous repair theory enriches construction strategies for orthopaedic biomaterials: a narrative review, Immater. Transl. 2 (4) (2021) 343–360.
[4] Y.S. Kim, M. Majid, A.J. Melchiorri, A.G. Mikos, Applications of decellularized extracellular matrix in bone and cartilage tissue engineering, Bioeng. Transl. Med. 4 (1) (2019) 83–95.
[5] A.H. Schmidt, Autologous bone graft: is it still the gold standard? Injury 52 (Suppl 2) (2021) S18–S22.
[6] P. Wang, X. Wang, X. Li, B. Wang, J. Chen, X. Tu, 3D printing of osteocytic Dll4 integrated with PCL for cell fate determination towards osteoblasts in vitro, Bio-Design and Manufacturing 5 (2022) 493–511. https://doi.org/10.1007/s42242-022-00196-1.
[7] H.W. Kang, S.J. Lee, I.K. Ko, C. Kengla, J.J. Yoo, A. Atala, A 3D bioprinting system to produce human-scale tissue constructs with structural integrity, Nat. Biotechnol. 34 (3) (2016) 312–319.
[8] S. Jiang, M. Wang, J. He, A review of biomimetic scaffolds for bone regeneration: toward a cell-free strategy, Bioeng. Transl. Med. 6 (2) (2021), e10206.
[9] C.L. Mummery, R.P. Davis, J.E. Krieger, Challenges in using stem cells for cardiac repair, Sci. Transl. Med. 2 (27) (2010) 27ps17.
[10] J.A. Burdick, R.L. Mauck, J.H. Gorman 3rd, R.C. Gorman, Acellular biomaterials: an evolving alternative to cell-based therapies, Sci. Transl. Med. 5 (176) (2013) 176ps4.
[11] B.S. Kim, S. Das, J. Jang, D.W. Cho, Decellularized extracellular matrix-based bioinks for engineering tissue- and organ-specific microenvironments, Chem. Rev. 120 (19) (2020) 10608–10661.
[12] H. Xia, X. Li, W. Gao, X. Fu, R.H. Fang, L. Zhang, K. Zhang, Tissue repair and regeneration with endogenous stem cells, Nat. Rev. Mater. 3 (7) (2018) 174–193.
[13] C.W. Cheng, L.D. Solorio, E. Alsberg, Decellularized tissue and cell-derived extracellular matrices as scaffolds for orthopaedic tissue engineering, Biotechnol. Adv. 32 (2) (2014) 462–484.
[14] B. Kim, R. Ventura, B.T. Lee, Functionalization of porous BCP scaffold by generating cell-derived extracellular matrix from rat bone marrow stem cells culture for bone tissue engineering, J. Tissue Eng. Regen Med. 12 (2) (2018) e1256–e1267.
[15] Y. Song, J. Soto, S. Li, Mechanical regulation of histone modifications and cell plasticity, Curr. Opin. Solid State Mater. Sci. 24 (6) (2020).
[16] M. Marinkovic, T.J. Block, R. Rakian, Q. Li, E. Wang, M.A. Reilly, D.D. Dean, X. D. Chen, One size does not fit all: developing a cell-specific niche for in vitro study of cell behavior, Matrix Biol. 52–54 (2016) 426–441.
[17] A. Voss, M.B. McCarthy, A. Hoberman, M.P. Cote, A.B. Imhoff, A.D. Mazzocca, K. Beitzel, Extracellular matrix of current biological scaffolds promotes the differentiation potential of mesenchymal stem cells, Arthroscopy 32 (11) (2016) 2381–2392.e1.
[18] T. Hoshiba, G. Chen, C. Endo, H. Maruyama, M. Wakui, E. Nemoto, N. Kawazoe, M. Tanaka, Decellularized extracellular matrix as an in vitro model to study the comprehensive roles of the ECM in stem cell differentiation, Stem Cell. Int. 2016 (2016), 6397820.
[19] Y. Mao, T. Hoffman, A. Wu, R. Goyal, J. Kohn, Cell type-specific extracellular matrix guided the differentiation of human mesenchymal stem cells in 3D polymeric scaffolds, J. Mater. Sci. Mater. Med. 28 (7) (2017) 100.
[20] F. Pati, T.H. Song, G. Rijal, J. Jang, S.W. Kim, D.W. Cho, Ornamenting 3D printed scaffolds with cell-laid extracellular matrix for bone tissue regeneration, Biomaterials 37 (2015) 230–241.
[21] S. Jiang, M. Wang, J. He, A review of biomimetic scaffolds for bone regeneration: toward a cell-free strategy, Bioeng. Transl. Med. 6 (2) (2020).
[22] W. Zhang, X. Zhang, S. Wang, L. Xu, M. Zhang, G. Wang, Y. Jin, X. Zhang, X. Jiang, Comparison of the use of adipose tissue-derived and bone marrow-derived stem cells for rapid bone regeneration, J. Dent. Res. 92 (12) (2013) 1136–1141.
[23] H. Lee, G.H. Yang, M. Kim, J. Lee, J. Huh, G. Kim, Fabrication of micro/nanoporous collagen/dECM/silk-fibroin biocomposite scaffolds using a low temperature 3D printing process for bone tissue regeneration, Mater. Sci. Eng. C. Mater. Biol. Appl. 84 (2018) 140–147.
[24] J. Ma, W. Guo, M. Gao, B. Huang, Q. Qi, Z. Ling, Y. Chen, H. Hu, H. Zhou, F. Yu, K. Chen, G. Richards, J. Lin, Z. Zhou, D. Xiao, X. Zou, Biomimetic matrix fabricated by LMP-1 gene-transduced MC3T3-E1 cells for bone regeneration, Biofabrication 9 (4) (2017), 045010.
[25] B. Aldemir Dikici, G.C. Reilly, F. Claeyssens, Boosting the osteogenic and angiogenic performance of multiscale porous polycaprolactone scaffolds by in vitro generated extracellular matrix decoration, ACS Appl. Mater. Interfaces 12 (11) (2020) 12510–12524.
[26] A. Salhotra, H. Shah, B. Levi, M. Longaker, Mechanisms of bone development and repair, Nature reviews, Mol. Cell Biol. 21 (11) (2020) 696–711.
[27] J. Xiong, M. Onal, R.L. Jilka, R.S. Weinstein, S.C. Manolagas, C.A. O'Brien, Matrix-embedded cells control osteoclast formation, Nat. Med. 17 (10) (2011) 1235–1241.
[28] T. Nakashima, M. Hayashi, T. Fukunaga, K. Kurata, M. Oh-Hora, J.Q. Feng, L. F. Bonewald, T. Kodama, A. Wutz, E.F. Wagner, J.M. Penninger, H. Takayanagi, Evidence for osteocyte regulation of bone homeostasis through RANKL expression, Nat. Med. 17 (10) (2011) 1231–1234.
[29] X. Tu, Y. Rhee, K.W. Condon, N. Bivi, M.R. Allen, D. Dwyer, M. Stolina, C. H. Turner, A.G. Robling, L.I. Plotkin, T. Bellido, Sost downregulation and local Wnt signaling are required for the osteogenic response to mechanical loading, Bone 50 (1) (2012) 209–217.
[30] B. Javaheri, A.R. Stern, N. Lara, M. Dallas, H. Zhao, Y. Liu, L.F. Bonewald, M. L. Johnson, Deletion of a single β-catenin allele in osteocytes abolishes the bone anabolic response to loading, J. Bone Miner. Res. 29 (3) (2014) 705–715.
[31] Y. Cui, P.J. Niziolek, B.T. MacDonald, C.R. Zylstra, N. Alenina, D.R. Robinson, Z. Zhong, S. Matthes, C.M. Jacobsen, R.A. Conlon, R. Brommage, Q. Liu, F. Mseeh, D.R. Powell, Q.M. Yang, B. Zambrowicz, H. Gerrits, J.A. Gossen, X. He, M. Bader, B. O. Williams, M.L. Warman, A.G. Robling, Lrp5 functions in bone to regulate bone mass, Nat. Med. 17 (6) (2011) 684–691.
[32] A.G. Robling, L.F. Bonewald, The osteocyte: new insights, Annu. Rev. Physiol. 82 (2020) 485–506.
[33] E. Jackson, N. Lara-Castillo, M.P. Akhter, M. Dallas, J.M. Scott, T. Ganesh, M. L. Johnson, Osteocyte Wnt/beta-catenin pathway activation upon mechanical loading is altered in ovariectomized mice, BoneKEy Rep. 15 (2021), 101129.
[34] Y. Liu, J. Fang, Q. Zhang, X. Zhang, Y. Cao, W. Chen, Z. Shao, S. Yang, D. Wu, M. Hung, Y. Zhang, W. Tong, H. Tian, Wnt10b-overexpressing umbilical cord mesenchymal stem cells promote critical size rat calvarial defect healing by enhanced osteogenesis and VEGF-mediated angiogenesis, J. Orthop. Transl. 23 (2020) 29–37.

[35] X. Tu, J. Delgado-Calle, K.W. Condon, M. Maycas, H. Zhang, N. Carlesso, M. M. Taketo, D.B. Burr, L.I. Plotkin, T. Bellido, Osteocytes mediate the anabolic actions of canonical Wnt/beta-catenin signaling in bone, Proc. Natl. Acad. Sci. U. S. A. 112 (5) (2015) E478–E486.
[36] J. Osório, Bone. Osteocyte-specific activation of the canonical Wnt-β catenin pathway stimulates bone formation, Nat. Rev. Endocrinol. 11 (4) (2015) 192.
[37] J. Buckland, Bone: anabolic Wnt/β-catenin signalling: osteocytes are key, Nat. Rev. Rheumatol. 11 (3) (2015) 128.
[38] J. Delgado-Calle, X. Tu, R. Pacheco-Costa, K. McAndrews, R. Edwards, G. G. Pellegrini, K. Kuhlenschmidt, N. Olivos, A. Robling, M. Peacock, L.I. Plotkin, T. Bellido, Control of bone anabolism in response to mechanical loading and PTH by distinct mechanisms downstream of the PTH receptor, J. Bone Miner. Res. 32 (3) (2017) 522–535.
[39] Y. Liu, X. Ruan, J. Li, B. Wang, J. Chen, X. Wang, P. Wang, X. Tu, The osteocyte stimulated by Wnt agonist SKL2001 is a safe osteogenic niche improving bioactivities in a polycaprolactone and cell integrated 3D module, Cells 11 (5) (2022) 831.
[40] M.J. Kratochvil, A.J. Seymour, T.L. Li, S.P. Pasca, C.J. Kuo, S.C. Heilshorn, Engineered materials for organoid systems, Nat. Rev. Mater. 4 (9) (2019) 606–622.
[41] N. Bivi, K. Condon, M. Allen, N. Farlow, G. Passeri, L. Brun, Y. Rhee, T. Bellido, L. Plotkin, Cell autonomous requirement of connexin 43 for osteocyte survival: consequences for endocortical resorption and periosteal bone formation, J. Bone Miner. Res. : Off. J. Am. Soc. Bone Min. Res. 27 (2) (2012) 374–389.
[42] N. Harada, Y. Tamai, T. Ishikawa, B. Sauer, K. Takaku, M. Oshima, M. Taketo, Intestinal polyposis in mice with a dominant stable mutation of the beta-catenin gene, EMBO J. 18 (21) (1999) 5931–5942.
[43] X. Tu, K.S. Joeng, K.I. Nakayama, K. Nakayama, J. Rajagopal, T.J. Carroll, A. P. McMahon, F. Long, Noncanonical Wnt signaling through G protein-linked PKCdelta activation promotes bone formation, Dev. Cell 12 (1) (2007) 113–127.
[44] A.R. Stern, M.M. Stern, M.E. Van Dyke, K. Jahn, M. Prideaux, L.F. Bonewald, Isolation and culture of primary osteocytes from the long bones of skeletally mature and aged mice, Biotechniques 52 (6) (2012) 361–373.
[45] K. Otero, M. Shinohara, H. Zhao, M. Cella, S. Gilfillan, A. Colucci, R. Faccio, F. Ross, S. Teitelbaum, H. Takayanagi, M. Colonna, TREM2 and β-catenin regulate bone homeostasis by controlling the rate of osteoclastogenesis, J. Immunol. 188 (6) (2012) 2612–2621.
[46] W. Xue, B. Krishna, A. Bandyopadhyay, S. Bose, Processing and biocompatibility evaluation of laser processed porous titanium, Acta Biomater. 3 (6) (2007) 1007–1018.
[47] J. Silva, M. Carvalho, R. Udangawa, C. Moura, J. Cabral, C. L da Silva, F. Ferreira, D. Vashishth, R. Linhardt, Extracellular matrix decorated polycaprolactone scaffolds for improved mesenchymal stem/stromal cell osteogenesis towards a patient-tailored bone tissue engineering approach, J. Biomed. Mater. Res., Part B 108 (5) (2020) 2153–2166.
[48] M. Deng, J. Tan, C. Hu, T. Hou, W. Peng, J. Liu, B. Yu, Q. Dai, J. Zhou, Y. Yang, R. Dong, C. Ruan, S. Dong, J. Xu, Modification of PLGA scaffold by MSC-derived extracellular matrix combats macrophage inflammation to initiate bone regeneration via TGF-beta-induced protein, Adv. Healthc Mater. 9 (13) (2020), e2000353.
[49] W. Guo, M. Chen, Z. Wang, Y. Tian, J. Zheng, S. Gao, Y. Li, Y. Zheng, X. Li, J. Huang, W. Niu, S. Jiang, C. Hao, Z. Yuan, Y. Zhang, M. Wang, Z. Wang, J. Peng, A. Wang, Y. Wang, X. Sui, W. Xu, L. Hao, X. Zheng, S. Liu, Q. Guo, 3D-printed cell-free PCL-MECM scaffold with biomimetic micro-structure and micro-environment to enhance in situ meniscus regeneration, Bioact. Mater. 6 (10) (2021) 3620–3633.
[50] F. Chowdhury, S. Na, D. Li, Y.C. Poh, T.S. Tanaka, F. Wang, N. Wang, Material properties of the cell dictate stress-induced spreading and differentiation in embryonic stem cells, Nat. Mater. 9 (1) (2010) 82–88.
[51] M. Schliwa, Action of cytochalasin D on cytoskeletal networks, J. Cell Biol. 92 (1) (1982) 79–91.
[52] J. Huang, D. Lin, Z. Wei, Q. Li, J. Zheng, Q. Zheng, L. Cai, X. Li, Y. Yuan, J. Li, Parathyroid hormone derivative with reduced osteoclastic activity promoted bone regeneration via synergistic bone remodeling and angiogenesis, Small 16 (6) (2020), e1905876.
[53] N. Shang, J. Wu, Egg white ovotransferrin attenuates RANKL-induced osteoclastogenesis and bone resorption, Nutrients 11 (9) (2019).
[54] E.H. Schemitsch, Size matters: defining critical in bone defect size, J. Orthop. Trauma 31 (Suppl 5) (2017) S20–s22.
[55] C. Cheng, V. Alt, A. Dimitrakopoulou-Strauss, L. Pan, U. Thormann, R. Schnettler, K. Weber, L. Strauss, Evaluation of new bone formation in normal and osteoporotic rats with a 3-mm femur defect: functional assessment with dynamic PET-CT (dPET-CT) using 2-deoxy-2-[(18)F]fluoro-D-glucose ((18)F-FDG) and (18)F-fluoride, Mol. Imag. Biol. 15 (3) (2013) 336–344.
[56] J. Brosch-Lenz, C. Uribe, A. Gosewisch, L. Kaiser, A. Todica, H. Ilhan, F. J. Gildehaus, P. Bartenstein, A. Rahmim, A. Celler, S. Ziegler, G. Böning, Influence of dosimetry method on bone lesion absorbed dose estimates in PSMA therapy: application to mCRPC patients receiving Lu-177-PSMA-I&T, EJNMMI Phys. 8 (1) (2021) 26.
[57] N. AlMuraikhi, D. Ali, A. Alshanwani, R. Vishnubalaji, M. Manikandan, M. Atteya, A. Siyal, M. Alfayez, A. Aldahmash, M. Kassem, N. Alajez, Stem cell library screen identified ruxolitinib as regulator of osteoblastic differentiation of human skeletal stem cells, Stem Cell Res. Ther. 9 (1) (2018) 319.
[58] S. Tetè, R. Vinci, S. Zara, V. Zizzari, A. Cataldi, F. Mastrangelo, C. Mortellaro, E. Gherlone, Atrophic jaw reconstruction by means of calvarial bone graft: long-term results, J. Craniofac. Surg. 21 (4) (2010) 1147–1152.
[59] L. Lei, Z. Liu, P. Yuan, R. Jin, X. Wang, T. Jiang, X. Chen, Injectable colloidal hydrogel with mesoporous silica nanoparticles for sustained co-release of microRNA-222 and aspirin to achieve innervated bone regeneration in rat mandibular defects, J. Mater. Chem. B 7 (16) (2019) 2722–2735.
[60] C. Qian, D. Tan, X. Wang, L. Li, J. Wen, M. Pan, Y. Li, W. Wu, J. Guo, Peripheral nerve injury-induced astrocyte activation in spinal ventral horn contributes to nerve regeneration, Neural Plast. 2018 (2018), 8561704.
[61] Y. Yan, H. Chen, H. Zhang, C. Guo, K. Yang, K. Chen, R. Cheng, N. Qian, N. Sandler, Y.S. Zhang, H. Shen, J. Qi, W. Cui, L. Deng, Vascularized 3D printed scaffolds for promoting bone regeneration, Biomaterials 190–191 (2019) 97–110.
[62] D.W. Hutmacher, Scaffolds in tissue engineering bone and cartilage, Biomaterials 21 (24) (2000) 2529–2543.
[63] S. Nagata, R. Hanayama, K. Kawane, Autoimmunity and the clearance of dead cells, Cell 140 (5) (2010) 619–630.
[64] J.M. Aamodt, D.W. Grainger, Extracellular matrix-based biomaterial scaffolds and the host response, Biomaterials 86 (2016) 68–82.
[65] A.B. Faia-Torres, M. Charnley, T. Goren, S. Guimond-Lischer, M. Rottmar, K. Maniura-Weber, N.D. Spencer, R.L. Reis, M. Textor, N.M. Neves, Osteogenic differentiation of human mesenchymal stem cells in the absence of osteogenic supplements: a surface-roughness gradient study, Acta Biomater. 28 (2015) 64–75.
[66] N.A. Sims, T.J. Martin, Osteoclasts provide coupling signals to osteoblast lineage cells through multiple mechanisms, Annu. Rev. Physiol. 82 (2020) 507–529.
[67] Y. Peng, S. Wu, Y. Li, J.L. Crane, Type H blood vessels in bone modeling and remodeling, Theranostics 10 (1) (2020) 426–436.
[68] W. Zhang, Y. Zhu, J. Li, Q. Guo, J. Peng, S. Liu, J. Yang, Y. Wang, Cell-derived extracellular matrix: basic characteristics and current applications in orthopedic tissue engineering, Tissue Eng. B Rev. 22 (3) (2016) 193–207.
[69] E.A. Aisenbrey, W.L. Murphy, Synthetic alternatives to matrigel, Nat. Rev. Mater. 5 (7) (2020) 539–551.
[70] C.P. Ng, A.R. Sharif, D.E. Heath, J.W. Chow, C.B. Zhang, M.B. Chan-Park, P. T. Hammond, J.K. Chan, L.G. Griffith, Enhanced ex vivo expansion of adult mesenchymal stem cells by fetal mesenchymal stem cell ECM, Biomaterials 35 (13) (2014) 4046–4057.
[71] M.L. Decaris, A. Mojadedi, A. Bhat, J.K. Leach, Transferable cell-secreted extracellular matrices enhance osteogenic differentiation, Acta Biomater. 8 (2) (2012) 744–752.
[72] Y. Fu, L. Liu, R. Cheng, W. Cui, ECM decorated electrospun nanofiber for improving bone tissue regeneration, Polymers 10 (3) (2018).
[73] Y.A. Wu, Y.C. Chiu, Y.H. Lin, C.C. Ho, M.Y. Shie, Y.W. Chen, 3D-Printed bioactive calcium silicate/poly-epsilon-caprolactone bioscaffolds modified with biomimetic extracellular matrices for bone regeneration, Int. J. Mol. Sci. 20 (4) (2019).
[74] M.S. Carvalho, J.C. Silva, J.M.S. Cabral, C.L. da Silva, D. Vashishth, Cultured cell-derived extracellular matrices to enhance the osteogenic differentiation and angiogenic properties of human mesenchymal stem/stromal cells, J. Tissue Eng. Regen Med. 13 (9) (2019) 1544–1558.
[75] M. Li, A. Zhang, J. Li, J. Zhou, Y. Zheng, C. Zhang, D. Xia, H. Mao, J. Zhao, Osteoblast/fibroblast coculture derived bioactive ECM with unique matrisome profile facilitates bone regeneration, Bioact. Mater. 5 (4) (2020) 938–948.
[76] Y. Yu, Y. Wang, W. Zhang, H. Wang, J. Li, L. Pan, F. Han, B. Li, Biomimetic periosteum-bone substitute composed of preosteoblast-derived matrix and hydrogel for large segmental bone defect repair, Acta Biomater. 113 (2020) 317–327.
[77] D.R. Haynes, T.N. Crotti, H. Zreiqat, Regulation of osteoclast activity in peri-implant tissues, Biomaterials 25 (20) (2004) 4877–4885.
[78] X. Chen, Z. Wang, N. Duan, G. Zhu, E.M. Schwarz, C. Xie, Osteoblast-osteoclast interactions, Connect. Tissue Res. 59 (2) (2018) 99–107.
[79] C.S. Bahney, R.L. Zondervan, P. Allison, A. Theologis, J.W. Ashley, J. Ahn, T. Miclau, R.S. Marcucio, K.D. Hankenson, Cellular biology of fracture healing, J. Orthop. Res. 37 (1) (2019) 35–50.
[80] S.G. Romeo, K.M. Alawi, J. Rodrigues, A. Singh, A.P. Kusumbe, S.K. Ramasamy, Endothelial proteolytic activity and interaction with non-resorbing osteoclasts mediate bone elongation, Nat. Cell Biol. 21 (4) (2019) 430–441.
[81] X. Liu, Y. Chai, G. Liu, W. Su, Q. Guo, X. Lv, P. Gao, B. Yu, G. Ferbeyre, X. Cao, M. Wan, Osteoclasts protect bone blood vessels against senescence through the angiogenin/plexin-B2 axis, Nat. Commun. 12 (1) (2021) 1832.
[82] Q. Ma, M. Liang, N. Limjunyawong, Y. Dan, J. Xing, J. Li, J. Xu, C. Dou, Osteoclast-derived apoptotic bodies show extended biological effects of parental cell in promoting bone defect healing, Theranostics 10 (15) (2020) 6825–6838.
[83] Y. Tang, X. Wu, W. Lei, L. Pang, C. Wan, Z. Shi, L. Zhao, T. Nagy, X. Peng, J. Hu, X. Feng, W. Van Hul, M. Wan, X. Cao, TGF-beta1-induced migration of bone mesenchymal stem cells couples bone resorption with formation, Nat. Med. 15 (7) (2009) 757–765.
[84] L. Xian, X. Wu, L. Pang, M. Lou, C. Rosen, T. Qiu, J. Crane, F. Frassica, L. Zhang, J. Rodriguez, Xiaofeng Jia, Shoshana Yakar, Shouhong Xuan, Argiris Efstratiadis, Mei Wan, Xu Cao, Matrix IGF-1 maintains bone mass by activation of mTOR in mesenchymal stem cells, Nat. Med. 18 (7) (2012) 1095–1101.
[85] L. Kreja, R. Brenner, A. Tautzenberger, A. Liedert, B. Friemert, C. Ehrnthaller, M. Huber-Lang, A. Ignatius, Non-resorbing osteoclasts induce migration and osteogenic differentiation of mesenchymal stem cells, J. Cell. Biochem. 109 (2) (2010) 347–355.
[86] M. Sanchez-Fernandez, A. Gallois, T. Riedl, P. Jurdic, B. Hoflack, Osteoclasts control osteoblast chemotaxis via PDGF-BB/PDGF receptor beta signaling, PLoS One 3 (10) (2008) e3537.
[87] X. Liu, Y. Sun, J. Shen, H. Min, J. Xu, Y. Chai, Strontium doped mesoporous silica nanoparticles accelerate osteogenesis and angiogenesis in distraction osteogenesis by activation of Wnt pathway, Nanomed. Nanotechnol. Biol. Med. 41 (2022), 102496.

[88] P.M. Crapo, T.W. Gilbert, S.F. Badylak, An overview of tissue and whole organ decellularization processes, Biomaterials 32 (12) (2011) 3233–3243.
[89] R. Londono, J.L. Dziki, E. Haljasmaa, N.J. Turner, C.A. Leifer, S.F. Badylak, The effect of cell debris within biologic scaffolds upon the macrophage response, J. Biomed. Mater. Res. 105 (8) (2017) 2109–2118.
[90] M. Li, T. Zhang, J. Jiang, Y. Mao, A. Zhang, J. Zhao, ECM coating modification generated by optimized decellularization process improves functional behavior of BMSCs, Mater. Sci. Eng. C. Mater. Biol. Appl. 105 (2019), 110039.
[91] S. Schwarz, L. Koerber, A.F. Elsaesser, E. Goldberg-Bockhorn, A.M. Seitz, L. Dürselen, A. Ignatius, P. Walther, R. Breiter, N. Rotter, Decellularized cartilage matrix as a novel biomatrix for cartilage tissue-engineering applications, Tissue Eng. 18 (21–22) (2012) 2195–2209.
[92] A.J. Sutherland, E.C. Beck, S.C. Dennis, G.L. Converse, R.A. Hopkins, C.J. Berkland, M.S. Detamore, Decellularized cartilage may be a chondroinductive material for osteochondral tissue engineering, PLoS One 10 (5) (2015), e0121966.
[93] L. Chen, C. Wu, D. Wei, S. Chen, Z. Xiao, H. Zhu, H. Luo, J. Sun, H. Fan, Biomimetic mineralized microenvironment stiffness regulated BMSCs osteogenic differentiation through cytoskeleton mediated mechanical signaling transduction, Mater. Sci. Eng. C. Mater. Biol. Appl. 119 (2021), 111613.
[94] T. Hoshiba, Cultured cell-derived decellularized matrices: a review towards the next decade, J. Mater. Chem. B 5 (23) (2017) 4322–4331.
[95] M. Rocco, M. Soligo, L. Manni, L. Aloe, Nerve growth factor: early studies and recent clinical trials, Curr. Neuropharmacol. 16 (10) (2018) 1455–1465.
[96] C. Kiecker, C. Niehrs, A morphogen gradient of Wnt/beta-catenin signalling regulates anteroposterior neural patterning in Xenopus, Development (Camb.) 128 (21) (2001) 4189–4201.
[97] W. Liu, Y. Luo, C. Ning, W. Zhang, Q. Zhang, H. Zou, C. Fu, Thermo-sensitive electroactive hydrogel combined with electrical stimulation for repair of spinal cord injury, J. Nanobiotechnol. 19 (1) (2021) 286.
[98] C. Anthony, D. Robbins, Y. Ahmed, E. Lee, Nuclear regulation of Wnt/β-catenin signaling: it's a complex situation, Genes 11 (8) (2020).
[99] R.S. Boneva, T.M. Folks, L.E. Chapman, Infectious disease issues in xenotransplantation, Clin. Microbiol. Rev. 14 (1) (2001) 1–14.